Narrow-band search for gravitational waves from known pulsars using the second LIGO observing run

LIGO Scientific Collaboration ; Virgo Collaboration ; et al ; Boetzel, Yannick ; Tiwari, Shubhanshu ; Haney, Maria

Abstract: Isolated spinning neutron stars, asymmetric with respect to their rotation axis, are expected to be sources of continuous gravitational waves. The most sensitive searches for these sources are based on accurate matched filtering techniques that assume the continuous wave to be phase locked with the pulsar beamed emission. While matched filtering maximizes the search sensitivity, a significant signal-to-noise ratio loss will happen in the case of a mismatch between the assumed and the true signal phase evolution. Narrow-band algorithms allow for a small mismatch in the frequency and spin-down values of the pulsar while coherently integrating the entire dataset. In this paper, we describe a narrow-band search using LIGO O2 data for the continuous wave emission of 33 pulsars. No evidence of a continuous wave signal is found, and upper limits on the gravitational wave amplitude over the analyzed frequency and spin-down ranges are computed for each of the targets. In this search, we surpass the spin-down limit, namely, the maximum rotational energy loss due to gravitational waves emission for some of the pulsars already present in the LIGO O1 narrow-band search, such as J1400−6325, J1813−1246, J1833−1034, J1952+3252, and for new targets such as J0940−5428 and J1747−2809. For J1400−6325, J1833−1034, and J1747−2809, this is the first time the spin-down limit is surpassed.

DOI: https://doi.org/10.1103/physrevd.99.122002

Narrow-band search for gravitational waves from known pulsars using the second LIGO observing run

B. P. Abbott *et al.*[*]
(LIGO Scientific Collaboration and Virgo Collaboration)

(Received 22 February 2019; published 27 June 2019)

Isolated spinning neutron stars, asymmetric with respect to their rotation axis, are expected to be sources of continuous gravitational waves. The most sensitive searches for these sources are based on accurate matched filtering techniques that assume the continuous wave to be phase locked with the pulsar beamed emission. While matched filtering maximizes the search sensitivity, a significant signal-to-noise ratio loss will happen in the case of a mismatch between the assumed and the true signal phase evolution. Narrow-band algorithms allow for a small mismatch in the frequency and spin-down values of the pulsar while coherently integrating the entire dataset. In this paper, we describe a narrow-band search using LIGO O2 data for the continuous wave emission of 33 pulsars. No evidence of a continuous wave signal is found, and upper limits on the gravitational wave amplitude over the analyzed frequency and spin-down ranges are computed for each of the targets. In this search, we surpass the spin-down limit, namely, the maximum rotational energy loss due to gravitational waves emission for some of the pulsars already present in the LIGO O1 narrow-band search, such as J1400 − 6325, J1813 − 1246, J1833 − 1034, J1952 + 3252, and for new targets such as J0940 − 5428 and J1747 − 2809. For J1400 − 6325, J1833 − 1034, and J1747 − 2809, this is the first time the spin-down limit is surpassed.

DOI: 10.1103/PhysRevD.99.122002

I. INTRODUCTION

Eleven gravitational wave (GW) signals have so far been detected by the LIGO [1,2] and Virgo GW interferometers [3] in their first and second observing runs (O1 and O2, respectively) [4]. All the signals detected so far come from the coalescence of two compact objects. These signals belong to the class of *transient signals*, since they are observed only within a short time window during the observing run. Ten detections of binary black hole mergers [4–9] and a detection from a binary neutron star (NS) merger [10] have been accomplished during the first and second observing runs.

Another class of GW signals potentially observable by the LIGO and Virgo detectors is the so-called *continuous wave* (CW). CWs could potentially be present during the entire data-taking period of the GW detectors. Potential sources of CWs are isolated spinning NSs asymmetric with respect to their rotation axis. In the case of an oblate NS, CWs are emitted at a frequency that is 2 times its rotational frequency.

Different types of CW searches can be performed according to the astrophysical scenario in which the NS is observed. If the NS is a pulsar, an accurate ephemeris may be available and matched filtering techniques can be employed to reach, ideally, the best possible sensitivity by using waveform templates that cover the entire observing run. These types of searches are referred to as *targeted searches*. The LIGO and Virgo Collaborations have already searched for this type of emission from known pulsars (both isolated and some in binaries) [11–19], for which accurate ephemerides were available. While for NSs observed as a central compact object of a supernova remnant or in a binary system, usually accurate ephemerides are not available. In this case, we can pinpoint the source and look for the CW signal over a wide frequency range using semicoherent analysis, e.g., dividing the observing run in several data chunks and looking for a waveform template in each of them. Such searches are called *"directed"* and offer the possibility to explore a large number of templates at the price of a lower sensitivity with respect to targeted searches [20–24]. Recently, there has also been a study for a possible deviation of CW signals from the general relativity model [25] by including non-tensorial modes.

Between targeted and directed searches, we find the *narrow-band* searches. Such pipelines are based on algorithms which allow us to make a full coherent search, and, at the same time, we are able to deal with a frequency mismatch between the CW signal and the electromagnetic inferred value of the order of 500 mHz [14,26,27]. Usually, this will correspond to the evaluation of millions of waveform templates for each pulsar considered in the analysis.

[*]Full author list given at the end of the article.

Hence, narrow-band searches offer a sensitivity comparable to the one of targeted searches while relaxing the phase-lock assumption of the CW signal with the NS rotation. The CW phase locking is indeed a strong assumption that may prevent the detection of a CW signal. In fact, a coherent (or targeted) CW search that uses one year of data has a frequency resolution of about 3×10^{-8} Hz. A mismatch between the rotational frequency inferred from the ephemeris and the CW signal frequency of this size or larger is enough to drastically reduce the chance of detection.

A small frequency mismatch may arise for several physical reasons that usually are parametrized in a frequency mismatch of the form $\Delta f_{\rm gw} \sim f_{\rm gw}(1+\delta)$ [14]. In the case of a differential rotation between the GW engine and the electromagnetic pulse engine, the factor δ will be proportional to the timescale of some torque which enforces correlation between the two engines. Another possibility is that the NS is freely precessing. In this scenario, the δ factor will be proportional to the angle between the star symmetry axis and the star rotation axis [28]. In some of the previous narrow-band searches [14,26], we used a value of $\delta \sim 10^{-4}$, which can accommodate the previous theoretical models. However starting from the first narrow-band search with advanced detector data [27], we explore a frequency/spin-down range corresponding to $\delta \sim 10^{-3}$.

Another possibility is that the pulsar ephemerides provided are not accurate enough to carry on targeted searches with the required resolution, or they are not available during the observing time of our detectors. That is the case for many low-frequency and energetic pulsars observed in the x- and γ-ray bands, such as J1833 − 1034 and J1813 − 1749. For these reasons, along with targeted searches, we search for CWs also with narrow-band searches.

In this paper, we present the narrow-band search for CWs from 33 known pulsars using LIGO O2 data. In Sec. II, we provide a brief background on the CW signal model and the algorithm used. In Sec. III, we summarize the main features of the O2 narrow-band analysis, while in Sec. IV, we introduce the pulsars that we have selected for this search. The results of the search followed by the upper limits on the signal strain amplitude are discussed in Sec. V. Finally, in Sec. VI we draw the conclusion of this work.

II. BACKGROUND

A. The signal

The GW signal emitted by an asymmetric spinning NS can be written at the detector frame using the formalism introduced in [29] as the real part of

$$h(t) = H_0(H^+(\eta,\psi)A_+(t) + H^\times(\eta,\psi)A_\times(t))e^{2\pi i f_{\rm gw}(t)t + i\phi_0}, \tag{1}$$

where $f_{\rm gw}(t)$ is the GW frequency (which incorporates all the modulation of the signal at the detector frame) and ϕ_0 an initial phase. The polarization amplitudes $H^+(\eta,\psi), H^\times(\eta,\psi)$ are functions of the ratio of the polarization ellipse semiminor to semimajor axis η and the polarization angle ψ. The functions $A_+(t), A_\times(t)$ are the detector responses to the two wave polarizations. These two functions depend on the detector geographical location and the $0, \pm 1, \pm 2$ harmonics of the sidereal rotational frequency of Earth $F_{\rm sid}$ (the inverse of the sidereal day); see [29] for more details. In Eq. (1), the amplitude of the GW H_0 is related to the canonical strain amplitude h_0 given the angle between the line of sight and the star rotation axis ι:

$$H_0 = h_0\sqrt{\frac{1+6\cos^2\iota+\cos^4\iota}{4}} \tag{2}$$

and

$$h_0 = \frac{1}{d}\frac{4\pi^2 G}{c^4} I_{zz} f_{\rm gw}^2 \epsilon, \tag{3}$$

with d, I_{zz}, and ϵ the star distance, moment of inertia with respect to the rotation axis, and *ellipticity*. The ellipticity measures the degree of asymmetry of the star with respect to its rotation axis. In the detector reference frame, the signal is modulated by several effects, the most important being the *Römer delay* (also called the barycentric correction) due to the detector motion given by Earth's orbital motion and rotation, with respect to the GW source. Moreover, the GW signal is also modulated by the source's intrinsic spin-down due to the rotational energy loss from the source. Given a measure of the pulsar rotational frequency $f_{\rm rot}$, its derivative $\dot{f}_{\rm rot}$, and distance d, the GW signal amplitude can be constrained, assuming that all the star's rotational energy is lost via gravitational radiation. This theoretical value, which is an upper limit on the rotational energy that can be emitted in GWs, is called the *spin-down limit* and is given by [30]

$$h_{\rm sd} = 8.06 \times 10^{-19} I_{38}^{1/2}\left[\frac{1\ \rm kpc}{d}\right]\left[\frac{\dot{f}_{\rm rot}}{\rm Hz/s}\right]^{1/2}\left[\frac{\rm Hz}{f_{\rm rot}}\right]^{1/2}, \tag{4}$$

where I_{38} is the star's moment of inertia in units of 10^{38} kg m^2. Different values of the moment of inertia are possible according to the NS equation of state, mass, and spin [31]; however, in this work we will assume its canonical value to be $I = 10^{38}$ kg m^2. The corresponding spin-down limit on the star's equatorial fiducial ellipticity can be obtained from Eq. (3),

$$\epsilon_{\rm sd} = 1.91 \times 10^{5} I_{38}^{-1/2}\left[\frac{\dot{f}_{\rm rot}}{\rm Hz/s}\right]^{1/2}\left[\frac{\rm Hz}{f_{\rm rot}}\right]^{5/2}, \tag{5}$$

which does not depend on the star's distance.

B. The five-vector narrow-band pipeline

The narrow-band pipeline uses the five-vector method [32] and, in particular, its latest implementation for narrow-band searches described in [33].

The pipeline explores a range of frequency and spin-down values by applying barycentric and spin-down corrections to the data and then identifies the GW signal using its characteristic frequency components.

The pipeline first removes the modulations given by the barycentric corrections and intrinsic source spin-down. The barycentric corrections are applied using a frequency-independent nonuniform resampling [33]. The spin-down is removed by applying a phase correction on the data time series. Also, the Einstein delay is corrected in the time domain.

Once we have removed the barycentric and spin-down modulations of a possible signal, the GW signal power is spread among five frequencies given by the coupling of the signal frequency and the detector sidereal responses $A_+(t), A_\times(t)$. These frequency components are $f_{\rm gw}-2F_{\rm sid}$, $f_{\rm gw}-F_{\rm sid}, f_{\rm gw}, f_{\rm gw}+F_{\rm sid}$, and $f_{\rm gw}+2F_{\rm sid}$, where $F_{\rm sid}$ is the frequency corresponding to the Earth sidereal day.

Hence, a pair of matched filters, one for each sidereal response function, is computed for each point of the explored parameter space. This is done using a frequency grid which allows us to compute the matched filters simultaneously over the whole analyzed frequency band. These steps are done separately for each detector. Then, the output of the matched filters at each point of the parameter space are combined, taking into account the phase shift[1] between the two datasets in order to build a detection statistic.

The next step consists of selecting the maximum of the detection statistic for every 10^{-4} Hz interval and over the whole spin-down range. Within this set, points in the parameter space with a p value below a 0.1% threshold (taking into account the number of trials) are considered as potentially interesting outliers and are subject to further analysis steps; see Appendix B for more details.

III. THE ANALYSIS

The LIGO second observing run O2 started on November 30, 2016 16:00:00 UTC and ended on August 25, 2017 22:00:00 UTC, while Virgo joined the run later on August 1, 2017 12:00:00 UTC and ended on August 25, 2017 22:00:00 UTC. The narrow-band search can be performed jointly between different detectors if the datasets cover the same observing time. Since Virgo O2 data covered just approximately one month at the end of O2 and was characterized by a lower sensitivity with respect to LIGO data, we have decided to exclude it from the analysis. For this analysis, we have used the second version of calibrated LIGO data (C02) [34]. We jointly analyzed LIGO Hanford (LHO) and LIGO Livingston (LLO) data over the period between January 4, 2017 00:00:00 UTC and August 25, 2017 22:00:00 UTC. LLO data between the beginning of the run and December 22, 2016 have been excluded due to bad spectral contamination, while both detectors underwent a commissioning break between December 22, 2016 and January 4, 2017. The observing time $T_{\rm obs}$ was ∼232 days, implying frequency and spin-down bins of, respectively, $\delta f = 5\times10^{-8}$ Hz and $\delta\dot{f} = 2.5\times10^{-15}$ Hz/s. LHO and LLO duty cycles were about 45% and 56% and corresponded to an effective observing time of 104 and 129 days, respectively.[2] The sensitivity of the O2 search is reported in Fig. 1, where we also show O1 sensitivity. While at lower frequency, only O2 LLO seems to be much better than O1, at higher frequencies the sensitivity is significantly better for both detectors. In order to validate the analysis, we have looked for four hardware injections in the data, checking if their parameters were recovered correctly; see Appendix A.

The explored frequency and spin-down ranges were set to 0.4% of the pulsar rotational frequency and spin-down reported in the ephemeris. Since in this analysis we subsampled data at 1 Hz, the explored frequency region of some pulsars has been chosen manually in order to avoid a possible signal aliasing.

We have decided to select as *outliers* for the follow-up the points in the parameter space with a value of the detection statistic corresponding to a p value of 0.1% (taking into account the number of trials) or smaller. In the previous O1 search, we used a threshold of 1% due to the fact that the data quality of LHO and LLO was significantly different at lower frequencies; see Appendix B for more details.

IV. SELECTED TARGETS

In our O2 analysis, we have selected as an initial set of targets all the pulsars present in the O1 narrow-band search [27]. Then, we have enlarged it, deciding to analyze all the pulsars with rotation frequency of 10 and 350 Hz with spin-down limit given in Eq. (4) within a factor of 10 from the optimal sensitivity of the search of O2 LLO (in most cases). This choice has been driven by the fact that available pulsar distances can be affected by a large error. The spin-down limit has been computed according to the most recent estimation of the distance given in the ATNF catalog [35] (v1.58) and extrapolating the rotational frequency and spin-down rate at the O2 epoch. For the pulsars J1028 − 5819, J1112 − 6103, J1813 − 1246, and J2043 + 2740, we have checked that the extrapolated rotational parameters together with the ranges explored in the narrow-band search cover

[1]This is given by the fact that the data sampling usually does not begin at the exact same time for different detectors.

[2]With the exception of pulsars that have glitched during the analysis. For those, we have performed two independent analyses before and after the glitch.

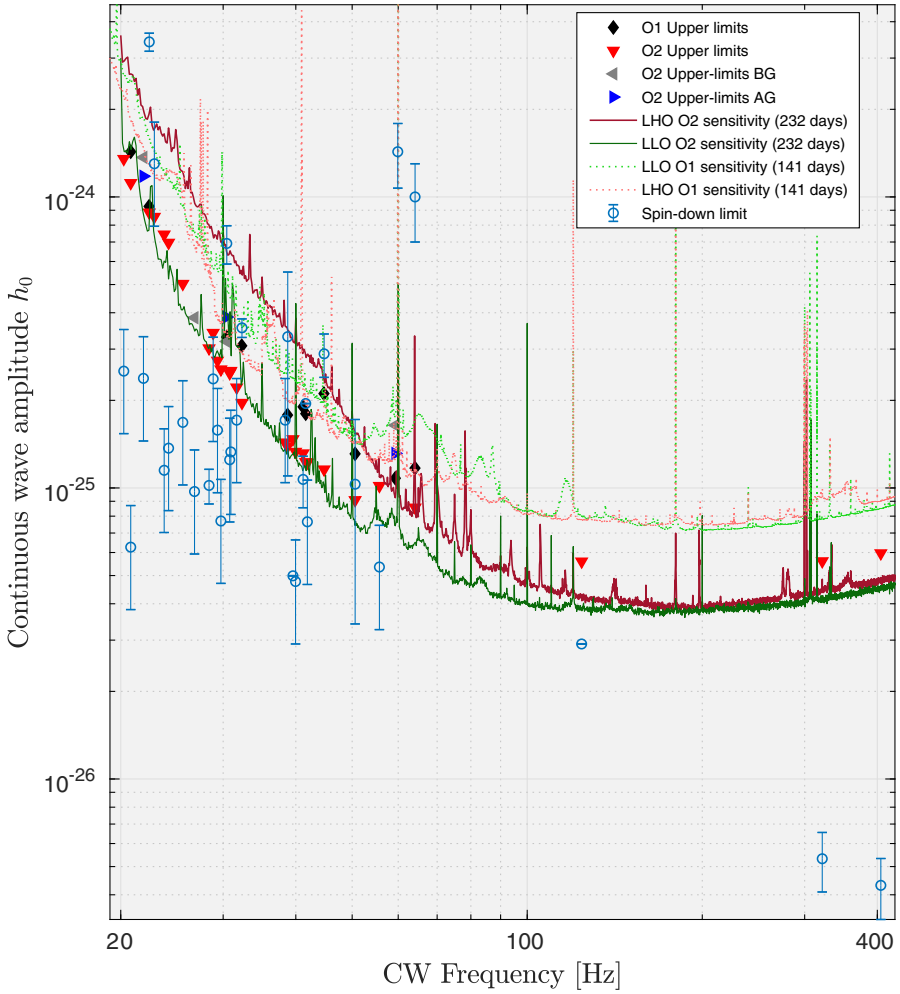

FIG. 1. Vertical axis: CW amplitude. Horizontal axis: Searched GW frequencies. The different lines indicate the estimated search sensitivity for O1 and O2 narrow-band searches, while the different markers indicate ULs. The labels "AG" and "BG" refer to a search performed after or before the glitch of a given pulsar. The error bars correspond to the uncertainties on the pulsar distance and correspond to 1σ confidence level.

the values reported by the updated ephemeris during the O2 epoch in [19]. For the pulsars J0835 − 4510, J0940−5428, J1105 − 6107, J1410 − 6132, J1420 − 6048, J1531−5610, J1718 − 3825, J1809 − 1917, and J1838 − 0655, the extrapolated spin-down rate resulted off range with respect to the one reported in [19], and for this reason, the searched parameter space has been adjusted in such a way to cover the updated values. For the pulsars J0205 + 6449, J0534 + 2200, J1913 + 1011, J1952 + 3252, and J2229 + 6114, we have used updated ephemerides provided by the telescopes at Jodrell Bank (UK). For the remaining pulsars, no monitoring is present during the O2 run. Even though we are aware that an extrapolation from outdated ephemerides might bring a GW search which does not cover the actual pulsar rotational parameters during O2, we have decided to carry on the analysis in such a way to exploit the possibility that the actual pulsar rotational parameters were covered even partially by the narrow-band search.

Table I reports the spin-down limit on amplitude h_0 and ellipticity ϵ for each target, given their distance estimation and uncertainty. Hereafter, the distance uncertainties are propagated to the derived quantities (such as the spin-down limit) assuming normal distributions, namely,

$$\sigma_Y^2 = \left(\frac{\partial Y}{\partial d}\right)^2 \sigma_d^2,$$

with Y being a function of the distance and σ^2 the distribution variance.

The spin-down limits are compared to the estimated narrow-band search sensitivity in Fig. 1. The analysis covers the 11 targets that we have already analyzed for O1 plus 22 new targets. Based on the estimated sensitivity, we expected to surpass the spin-down limit in the O2 analysis for nine of the 11 O1 targets. The exceptions are J2043 + 2740 and J2229 + 6114, for which the current distance estimation has been increased with respect to the ATNF catalog v1.54 (the catalog used for O1 [27]).

TABLE I. Properties of analyzed pulsars. The second column reports the distance as provided by the ephemerides based on the dispersion measure and the galactic electron density model of [36]. If the pulsar distance is estimated according to an independent measure, we refer to it next to the name entry. The distance uncertainty refers to 1σ confidence level and is assumed to have a normal distribution. In the third and fourth columns, the spin-down limit $h_{\rm sd}$ and the corresponding ellipticity $\epsilon_{\rm sd}$ are computed using Eqs. (4) and (5).

Name	d (kpc)	$h_{\rm sd}$	$\epsilon_{\rm sd}$
J0205 + 6449 [37]	2.0 ± 0.3	$(6.9 \pm 1.1) \times 10^{-25}$	1.42×10^{-3}
J0534 + 2200 [38]	2.0 ± 0.5	$(1.4 \pm 0.4) \times 10^{-24}$	7.56×10^{-4}
J0537 − 6910 [39]	49.7 ± 0.2	$(2.91 \pm 0.02) \times 10^{-26}$	8.90×10^{-5}
J0540 − 6919 [39]	49.7 ± 0.2	$(4.99 \pm 0.02) \times 10^{-26}$	1.50×10^{-3}
J0835 − 4510 [40]	0.28 ± 0.02	$(3.4 \pm 0.3) \times 10^{-24}$	1.80×10^{-3}
J0940 − 5428	0.4 ± 0.2	$(1.3 \pm 0.5) \times 10^{-24}$	8.97×10^{-4}
J1028 − 5819	1.4 ± 0.6	$(2.4 \pm 1.0) \times 10^{-25}$	6.70×10^{-4}
J1105 − 6107	2.4 ± 0.9	$(1.7 \pm 0.7) \times 10^{-25}$	3.82×10^{-4}
J1112 − 6103	4.5 ± 1.8	$(1.3 \pm 0.5) \times 10^{-25}$	5.61×10^{-4}
J1300 + 1240 [41]	0.7 ± 0.2	$(5.3 \pm 1.3) \times 10^{-27}$	3.17×10^{-8}
J1302 − 6350	2.3 ± 0.9	$(7.6 \pm 3.0) \times 10^{-26}$	9.52×10^{-5}
J1400 − 6325 [42]	0.9 ± 0.3	$(1.0 \pm 0.3) \times 10^{-24}$	2.07×10^{-4}
J1410 − 6132	13.5 ± 5.3	$(4.8 \pm 1.9) \times 10^{-26}$	3.83×10^{-4}
J1420 − 6048	5.6 ± 2.2	$(1.6 \pm 0.7) \times 10^{-25}$	9.81×10^{-4}
J1524 − 5625	3.4 ± 1.3	$(1.7 \pm 0.7) \times 10^{-25}$	8.25×10^{-4}
J1531 − 5610	2.8 ± 1.1	$(1.2 \pm 0.5) \times 10^{-25}$	5.47×10^{-4}
J1617 − 5055	4.7 ± 1.9	$(2.4 \pm 1.0) \times 10^{-25}$	1.28×10^{-3}
J1718 − 3825	3.5 ± 1.4	$(9.7 \pm 3.8) \times 10^{-26}$	4.48×10^{-4}
J1747 − 2809	8.2 ± 3.2	$(1.7 \pm 0.7) \times 10^{-25}$	8.97×10^{-4}
J1747 − 2958	2.5 ± 1.0	$(2.5 \pm 1.0) \times 10^{-25}$	1.47×10^{-3}
J1809 − 1917	3.3 ± 1.3	$(1.4 \pm 0.6) \times 10^{-25}$	7.27×10^{-4}
J1811 − 1925	5.0 ± 2.0	$(1.3 \pm 0.6) \times 10^{-25}$	6.59×10^{-4}
J1813 − 1246 [43]	> 2.5	$< 1.9 \times 10^{-25}$	2.67×10^{-4}
J1813 − 1749 [44]	4.7 ± 0.8	$(2.9 \pm 0.5) \times 10^{-25}$	6.42×10^{-4}
J1831 − 0952	3.7 ± 1.5	$(7.7 \pm 3.0) \times 10^{-26}$	3.04×10^{-4}
J1833 − 1034 [45]	4.1 ± 0.3	$(3.6 \pm 0.3) \times 10^{-25}$	1.32×10^{-3}
J1838 − 0655 [46]	6.6 ± 0.9	$(1.0 \pm 0.2) \times 10^{-25}$	7.94×10^{-4}
J1913 + 1011	4.6 ± 1.8	$(5.4 \pm 2.1) \times 10^{-26}$	7.54×10^{-5}
J1952 + 3252 [41]	3.0 ± 2.0	$(1.0 \pm 0.7) \times 10^{-25}$	1.15×10^{-4}
J2022 + 3842 [47]	10.0 ± 2.0	$(1.1 \pm 0.3) \times 10^{-25}$	6.00×10^{-4}
J2043 + 2740	1.5 ± 0.6	$(6.3 \pm 2.5) \times 10^{-26}$	2.03×10^{-4}
J2124 − 3358 [48]	0.4 ± 0.1	$(4.3 \pm 1.0) \times 10^{-27}$	9.49×10^{-9}
J2229 + 6114 [49]	3.0 ± 2.0	$(3.3 \pm 2.3) \times 10^{-25}$	6.27×10^{-4}

The new O2 targets mainly consist of pulsars with rotational frequencies within 10 and 20 Hz with spin-down rate $< -10^{-12}$ Hz/s, but there are also a few millisecond pulsars, for which we can approach the spin-down limit. Among these, there is the millisecond pulsar J2124 + 3358, for which we expect to barely approach the spin-down limit with targeted searches. One of these millisecond pulsars J1300 + 1240 is located in a binary system. However, according to the orbital parameters in the ephemeris, the intrinsic binary orbital modulation on a possible CW signal would be of the order of $\Delta f_{\rm bin} \approx 10^{-10}$ Hz, which is below our frequency resolution and hence can be neglected.[3]

Millisecond pulsars are characterized by a low rotational spin-down value $\dot{f}_{\rm rot}$ together with a high rotational frequency $f_{\rm rot}$; hence, according to Eq. (4), their spin-down limit will also be harder to surpass our search sensitivities. Although the narrow-band search is currently not sensitive enough for the millisecond pulsars, we have decided to perform the search in order to test the capabilities of the pipeline at higher frequencies. Furthermore, pulsars J0205 + 6449, J0534 + 2200, J0835 − 4510, J1028 − 5819, and J1718 − 3825 had a glitch during O2. J0205 + 6449 glitched on May 27, 2017, J0534 + 2200 glitched on March 27, 2017, J0835 − 4510 had a glitch on December 16, 2016 [51], J1028 − 5819 glitched on May 29, 2017, and J1718 − 3825 glitched on May 1 July 2017 [19]. For these pulsars, we have performed two independent analyses, one before and one after the glitch, excluding

[3]The frequency shift due to the binary motion has been computed using [50].

TABLE II. First column: Pulsar name. Second and third columns: Central frequency and frequency width explored in the search. Fourth and fifth columns: Central spin-down and spin-down ranges explored in the search. Sixth and seventh columns: Number of templates in frequency and spin-down. Frequency and spin-down resolutions are, respectively, $\delta f \sim 5 \times 10^{-8}$ Hz, $\delta \dot{f} \sim 2.5 \times 10^{-15}$ Hz/s. The labels "AG" and "BG" indicate, respectively, after and before the glitch. Note that the frequency and spin-down resolution, and hence, the number of templates, are lower in the case of pulsars with a glitch.

Name	f (Hz)	Δf (Hz)	$\dot{f}$ (Hz/s)	$\Delta \dot{f}$ (Hz/s)	n_f (10^6)	$n_{\dot{f}}$
J0205 + 6449 AG	30.41	0.06	-8.61×10^{-11}	2.72×10^{-13}	0.47	17
J0205 + 6449 BG	30.41	0.06	-8.61×10^{-11}	2.44×10^{-13}	0.74	37
J0534 + 2200 AG	59.30	0.12	-7.38×10^{-10}	1.50×10^{-12}	1.53	251
J0534 + 2200 BG	59.30	0.12	-7.38×10^{-10}	1.56×10^{-12}	0.82	75
J0537 − 6910	123.86	0.25	-3.92×10^{-10}	8.01×10^{-13}	4.95	321
J0540 − 6919	39.39	0.08	-3.71×10^{-10}	7.56×10^{-13}	1.57	303
J0835 − 4510	22.37	0.04	-3.22×10^{-11}	8.51×10^{-14}	0.89	35
J0940 − 5428	22.84	0.05	-8.56×10^{-12}	2.50×10^{-14}	0.91	11
J1028 − 5819 AG	21.88	0.04	-3.86×10^{-12}	3.56×10^{-14}	0.33	3
J1028 − 5819 BG	21.88	0.04	-3.86×10^{-12}	2.63×10^{-14}	0.54	5
J1105 − 6107	31.64	0.06	-7.94×10^{-12}	2.00×10^{-14}	1.26	9
J1112 − 6103	30.78	0.06	-1.49×10^{-11}	3.50×10^{-14}	1.23	15
J1300 + 1240	321.62	0.64	-5.91×10^{-15}	5.00×10^{-15}	12.86	3
J1302 − 6350	41.87	0.08	-2.00×10^{-12}	5.00×10^{-15}	1.67	3
J1400 − 6325	64.12	0.13	-8.00×10^{-11}	1.65×10^{-13}	2.56	67
J1410 − 6132	39.95	0.08	-2.52×10^{-11}	7.01×10^{-14}	1.60	29
J1420 − 6048	29.32	0.06	-3.57×10^{-11}	1.00×10^{-13}	1.17	41
J1524 − 5625	25.56	0.05	-1.27×10^{-11}	3.00×10^{-14}	1.02	13
J1531 − 5610	23.75	0.05	-3.88×10^{-12}	1.50×10^{-14}	0.95	7
J1617 − 5055	28.80	0.06	-5.62×10^{-11}	1.15×10^{-13}	1.15	47
J1718 − 3825 BG	26.78	0.05	-4.72×10^{-12}	1.72×10^{-14}	0.82	5
J1747 − 2809	38.32	0.08	-1.14×10^{-10}	2.35×10^{-13}	1.53	95
J1747 − 2958	20.23	0.04	-1.25×10^{-11}	3.00×10^{-14}	0.81	13
J1809 − 1917	24.17	0.05	-7.44×10^{-12}	2.00×10^{-14}	0.97	9
J1811 − 1925	30.91	0.06	-2.10×10^{-11}	4.50×10^{-14}	1.23	19
J1813 − 1246	41.60	0.08	-1.52×10^{-11}	3.50×10^{-14}	1.66	15
J1813 − 1749	44.71	0.09	-1.27×10^{-10}	2.60×10^{-13}	1.79	105
J1831 − 0952	29.73	0.06	-3.67×10^{-12}	1.00×10^{-14}	1.19	5
J1833 − 1034	32.29	0.06	-1.05×10^{-10}	2.15×10^{-13}	1.29	87
J1838 − 0655	28.36	0.06	-1.99×10^{-11}	5.51×10^{-14}	1.13	23
J1913 + 1011	55.69	0.11	-5.25×10^{-12}	1.50×10^{-14}	2.23	7
J1952 + 3252	50.59	0.10	-7.48×10^{-12}	2.00×10^{-14}	2.02	9
J2022 + 3842	41.16	0.08	-7.30×10^{-11}	1.50×10^{-13}	1.64	61
J2043 + 2740	20.80	0.04	-2.75×10^{-13}	5.00×10^{-15}	0.83	3
J2124 − 3358	405.59	0.81	-16.92×10^{-16}	5.00×10^{-15}	16.21	3
J2229 + 6114	38.71	0.08	-5.84×10^{-11}	1.20×10^{-13}	1.55	49

the day in which the glitch was present. For J0835 − 4510 and J1718 − 3825, only the analysis after or before the glitch was done, since few data were available before or after the two glitches.

Table II reports the frequency/spin-down regions that we have analyzed for each of the 33 targets. The reference time for the rotational parameters of the pulsars is December 1, 2016 00:00:00 UTC.

V. RESULTS

The search has produced a total of 49 outliers for 15 of the 33 targets. Every outlier underwent a chain of follow-up steps aimed to test its nature, namely, (i) check for the presence of known instrumental noise lines, (ii) compare the SNR GW amplitude estimation among several detectors, and (iii) study the outlier significance with software injections. The outliers are given in Table III together with the follow-up step where we excluded them.

The narrow-band search carried out in the past on O1 data [27] produced two interesting outliers for J0835 − 4510 and 1833 − 1034. In order to confirm or reject them, the data from the first four months of O2 (available with calibration version C01 at the time) were used and no evidence of a signal was found. The full O2 analysis discussed in this paper confirms those findings. No outlier

TABLE III. This table summarizes the outliers found in the O2 narrow-band search. The first column reports the name of the pulsar for which we have found outliers. The second column gives the central frequency of the pulsar search band, and the third column the p value of the least significant outlier. The last column reports the step of the follow-up in which we have vetoed the outliers. For a description of the follow-up steps, refer to the main text.

Name	f	Number of outliers	p value	Step
J1105 − 6107	31.64	16[a]	4.23×10^{-4}	i,ii
J1112 − 6103	30.78	1[b]	1.83×10^{-4}	ii
J1300 + 1240	321.62	1	7.80×10^{-4}	iii
J1302 − 6350	41.87	4[c]	7.79×10^{-4}	ii
J1420 − 6048	29.32	11[d]	9.82×10^{-4}	i,ii
J1531 − 5610	23.75	1	4.65×10^{-4}	ii
J1617 − 5055	28.80	2	7.80×10^{-4}	ii,iii
J1747 − 2809	38.32	1	9.68×10^{-4}	ii
J1811 − 1925	30.91	1	3.30×10^{-4}	ii
J1813 − 1246	41.60	2[e]	6.73×10^{-4}	ii,iii
J1831 − 0952	29.73	1	2.15×10^{-4}	ii
J1833 − 1034	32.29	1	9.33×10^{-4}	ii
J1952 + 3252	50.59	4[f]	4.48×10^{-4}	i,ii
J2124 − 3358	405.59	2[g]	5.61×10^{-4}	i,iii
J2229 + 6114	38.71	1	9.66×10^{-4}	ii

[a]Most vetoed since they are close to the comb line of the 0.987925 Hz comb in LLO and the comb line of 2.109223 Hz in LHO.
[b]Various unidentified lines around 35.51 Hz.
[c]Unidentified noise disturbance in LHO at 41.8838 Hz.
[d]Comb of 1.945501 Hz in LHO.
[e]Unidentified broad line disturbance at 41.654–41.660 Hz.
[f]Comb of 2.109223 Hz in LHO, comb of 1.9455045 Hz in LHO, comb of 1.945437 Hz in LHO.
[g]Comb of 0.9967943 Hz in LLO.

has been found for J0835 − 4510, while an outlier has been found for J1833 − 1034, at a slightly different frequency which, however, as discussed in the next section, has been vetoed.

A. Outliers follow-up

The first step of the follow-up was to check if a known instrumental noise line was present in one of the two detectors [52]. This ruled out most of the candidates for the pulsars J1105 − 6107 and J2121 − 3358; see Appendix C for more details.

The second step of the follow-up was to study the evolution of the recovered signal-to-noise ratio (SNR) and amplitude h_0 with respect to the fraction of data samples that we were integrating. We expect the SNR to increase as the square root of the integration time and the amplitude h_0 to be nearly constant. We have performed this type of test in a LHO, LLO, and joint search for different integration times, checking if the SNR and h_0 estimation were compatible across the different cases.

Many outliers at frequencies <100 Hz have been classified as LHO disturbances since they have been observed only in LHO (see Appendix C). Some of these are in proximity of unidentified noise lines (lines which are confidently classified as detector disturbances but whose origin is unknown). That is the case of the outliers from J1112 − 6103, J1302 − 6350, and J1813 − 1246. Other outliers at low frequency were not in proximity to unidentified noise lines but have been vetoed as the signal-to-noise ratio is bigger than 8 only in LHO data, which has a sensitivity 2 to 3 times worse than LLO, thus, being incompatible with a true CW signal.

Only three outliers survived up to the third step of the follow-up, namely, from pulsars J1300 + 1240, J1617− 5055, and J2124 − 3358. For all these pulsars. we cannot approach the theoretical spin-down limit with our current search sensitivity, and this is a strong hint of the noise origin of these outliers. The last step of the follow-up consisted of studying the SNR and recovered CW amplitude h_0 with software injections with an amplitude h_0 fixed to that estimated for the outlier. The evolution of the SNR and h_0 for the outlier are then compared to the distributions derived from the injections. If they are compatible among the three different analyses, LHO, LLO, and joint combination, the outlier is subject to more dedicated studies. The two remaining outliers for the millisecond pulsars were ruled out since they were present in just one detector, while the injections predicted that they would be visible in both detectors. The J1617 − 5055 remaining outlier was also ruled out, as the injections show that they were likely driven by a LHO disturbance. Refer to Appendix C for more details on the last steps of this follow-up.

B. Upper limits

Since there was no evidence of the presence of a CW signal, we have computed upper limits (ULs) on the CW amplitude h_0. The ULs have been produced using the same procedure as in the O1 narrow-band search [27], which consists of injecting nonoverlapping GW signals with fixed amplitude h_0 in data every 10^{-4} Hz intervals. When 95% of injections produce a value of the detection statistic higher than the one used for the outlier selection, we set the upper limit to the injected amplitude value.

Figure 1 shows the median value of the UL for each of the 33 targets. The ULs are driven at lower frequencies by LLO sensitivity since it is the most sensitive detector in that frequency region. On the other hand, at higher frequencies, the ULs lie close to the sensitivity of the two detectors, which are indeed similar.

Table IV summarizes our results of the O2 narrow-band search. The table reports the median value of the UL on the strain amplitude h_0 and the corresponding ellipticity computed using Eq. (5). We consider the spin-down limit surpassed for a given pulsar if the ULs are lower than the spin-down limit over the entire frequency band.

The most stringent ULs have been set for the three pulsars J0537 − 6910, J1300 + 1240, and J2124 − 3358

TABLE IV. Upper limits summary table. First column: Pulsar name. Second and third columns: Median of the 95% confidence level UL on the GW amplitude h_0 and corresponding ellipticity ϵ. Fourth column: Surface deformation corresponding to the median ellipticity for a NS with radius of 10 km [53]. Fifth column: Ratio between the median UL and the spin-down limit. Sixth column: Ratio between the median UL on the GW and rotational energy losses. Last column: Minimum and maximum ratio between the ULs and the theoretical spin-down limit over the analyzed frequency/spin-down region. All the entries that use information on the astrophysical distance also include the corresponding uncertainty at 1σ confidence level.

Name	$\langle h\rangle_{\mathrm{UL}}$	$\langle\epsilon\rangle_{\mathrm{UL}}$	r_ϵ (cm)	$\langle h\rangle_{\mathrm{UL}}/h_{\mathrm{sd}}$	$\langle\dot{E}_{\mathrm{UL}}\rangle/\dot{E}_{\mathrm{sd}}$	$\min_{\mathrm{nb}}(\langle h\rangle_{\mathrm{UL}}/h_{\mathrm{sd}}) - \max_{\mathrm{nb}}(\langle h\rangle_{\mathrm{UL}}/h_{\mathrm{sd}})$
J0205 + 6449 AG	3.87×10^{-25}	$(7.9 \pm 1.2) \times 10^{-4}$	197.9	0.56 ± 0.08	0.3	$0.48^{+0.07}_{-0.07} - 0.67^{+0.10}_{-0.10}$
J0205 + 6449 BG	3.19×10^{-25}	$(6.5 \pm 1.0) \times 10^{-4}$	163.1	0.46 ± 0.07	0.2	$0.31^{+0.05}_{-0.05} - 0.58^{+0.09}_{-0.09}$
J0534 + 2200 AG	1.31×10^{-25}	$(7.1 \pm 1.8) \times 10^{-5}$	17.4	0.09 ± 0.02	0.008	$0.07^{+0.02}_{-0.02} - 0.11^{+0.03}_{-0.03}$
J0534 + 2200 BG	1.64×10^{-25}	$(8.8 \pm 2.2) \times 10^{-5}$	21.7	0.11 ± 0.03	0.01	$0.09^{+0.02}_{-0.02} - 0.14^{+0.03}_{-0.03}$
J0537 − 6910	5.59×10^{-26}	$(1.7 \pm 0.01) \times 10^{-4}$	⋯	1.92 ± 0.01	⋯	$1.13^{+0.00}_{-0.00} - 2.25^{+0.01}_{-0.01}$
J0540 − 6919	1.47×10^{-25}	$(4.43 \pm 0.02) \times 10^{-3}$	⋯	2.95 ± 0.01	⋯	$1.83^{+0.01}_{-0.01} - 3.47^{+0.02}_{-0.02}$
J0835 − 4510	8.82×10^{-25}	$(4.7 \pm 0.4) \times 10^{-4}$	116.8	0.26 ± 0.02	0.07	$0.14^{+0.01}_{-0.01} - 0.31^{+0.02}_{-0.02}$
J0940 − 5428	8.55×10^{-25}	$(5.9 \pm 2.3) \times 10^{-4}$	147.6	0.7 ± 0.3	0.5	$0.4^{+0.2}_{-0.2} - 0.8^{+0.4}_{-0.4}$
J1028 − 5819 AG	1.18×10^{-24}	$(3.3 \pm 1.3) \times 10^{-3}$	⋯	5.0 ± 2.0	⋯	$4.2^{+1.7}_{-1.7} - 6.0^{+2.3}_{-2.3}$
J1028 − 5819 BG	1.37×10^{-24}	$(3.8 \pm 1.5) \times 10^{-3}$	⋯	5.7 ± 2.3	⋯	$4.3^{+1.7}_{-1.7} - 7.0^{+2.7}_{-2.7}$
J1105 − 6107	2.20×10^{-25}	$(5.0 \pm 2.0) \times 10^{-4}$	123.0	1.3 ± 0.6	1.7	$0.68^{+0.3}_{-0.3} - 1.88^{+0.8}_{-0.8}$
J1112 − 6103	2.48×10^{-25}	$(1.1 \pm 0.5) \times 10^{-3}$	⋯	2.0 ± 0.8	⋯	$1.1^{+0.5}_{-0.5} - 2.5^{+1.0}_{-1.0}$
J1300 + 1240	5.60×10^{-26}	$(3.3 \pm 0.8) \times 10^{-7}$	⋯	10.5 ± 2.5	⋯	$6.3^{+1.5}_{-1.5} - 13.1^{+3.1}_{-3.1}$
J1302 − 6350	1.22×10^{-25}	$(1.5 \pm 0.6) \times 10^{-4}$	38.0	1.6 ± 0.7	2.6	$0.7^{+0.3}_{-0.3} - 1.9^{+0.8}_{-0.8}$
J1400 − 6325	8.57×10^{-26}	$(1.8 \pm 0.6) \times 10^{-5}$	4.4	0.09 ± 0.03	0.008	$0.05^{+0.01}_{-0.01} - 0.10^{+0.03}_{-0.03}$
J1410 − 6132	1.33×10^{-25}	$(1.1 \pm 0.5) \times 10^{-3}$	⋯	2.8 ± 1.1	⋯	$1.4^{+0.6}_{-0.6} - 3.5^{+1.4}_{-1.4}$
J1420 − 6048	2.75×10^{-25}	$(1.7 \pm 0.7) \times 10^{-3}$	426.8	1.7 ± 0.7	3.1	$0.9^{+0.4}_{-0.4} - 2.2^{+0.9}_{-0.9}$
J1524 − 5625	5.03×10^{-25}	$(2.5 \pm 1.0) \times 10^{-3}$	⋯	3.0 ± 1.2	⋯	$1.7^{+0.7}_{-0.7} - 3.7^{+1.5}_{-1.5}$
J1531 − 5610	7.51×10^{-25}	$(3.6 \pm 1.4) \times 10^{-3}$	⋯	6.5 ± 2.6	⋯	$3.7^{+1.5}_{-1.5} - 7.7^{+3.1}_{-3.1}$
J1617 − 5055	3.41×10^{-25}	$(1.8 \pm 0.6) \times 10^{-3}$	461.0	1.5 ± 0.6	2.1	$0.8^{+0.3}_{-0.3} - 1.8^{+0.8}_{-0.8}$
J1718 − 3825 BG	3.88×10^{-25}	$(1.8 \pm 0.7) \times 10^{-3}$	⋯	4.0 ± 1.6	⋯	$2.5^{+1.0}_{-1.0} - 4.8^{+2.0}_{-2.0}$
J1747 − 2809	1.43×10^{-25}	$(7.5 \pm 2.9) \times 10^{-4}$	188.1	0.8 ± 0.4	0.6	$0.5^{+0.2}_{-0.2} - 1.0^{+0.4}_{-0.4}$
J1747 − 2958	1.35×10^{-24}	$(7.9 \pm 3.1) \times 10^{-3}$	⋯	5.4 ± 2.1	⋯	$3.2^{+1.3}_{-1.3} - 6.7^{+2.6}_{-2.6}$
J1809 − 1917	6.95×10^{-25}	$(3.7 \pm 1.5) \times 10^{-3}$	⋯	5.1 ± 2.0	⋯	$3.1^{+1.2}_{-1.2} - 6.2^{+2.4}_{-2.4}$
J1811 − 1925	2.53×10^{-25}	$(1.2 \pm 0.5) \times 10^{-3}$	⋯	1.9 ± 0.8	⋯	$1.3^{+0.5}_{-0.5} - 2.3^{+0.9}_{-0.9}$
J1813 − 1246	1.23×10^{-25}	$\leq 7 \times 10^{-4}$	42.0	≥ 0.7	≥ 0.5	$\geq (0.4 - 0.8)$
J1813 − 1749	1.16×10^{-25}	$(2.6 \pm 0.5) \times 10^{-4}$	64.5	0.40 ± 0.07	0.2	$0.25^{+0.04}_{-0.04} - 0.49^{+0.08}_{-0.08}$
J1831 − 0952	2.56×10^{-25}	$(1.0 \pm 0.4) \times 10^{-3}$	⋯	3.3 ± 1.3	⋯	$2.1^{+0.9}_{-0.9} - 4.2^{+1.7}_{-1.7}$
J1833 − 1034	1.96×10^{-25}	$(7.3 \pm 0.6) \times 10^{-4}$	182.5	0.55 ± 0.04	0.3	$0.35^{+0.03}_{-0.03} - 0.71^{+0.05}_{-0.05}$
J1838 − 0655	3.03×10^{-25}	$(2.4 \pm 0.4) \times 10^{-3}$	⋯	3.0 ± 0.4	⋯	$1.8^{+0.3}_{-0.3} - 3.6^{+0.5}_{-0.5}$
J1913 + 1011	1.02×10^{-25}	$(1.4 \pm 0.6) \times 10^{-4}$	⋯	1.9 ± 0.8	⋯	$1.1^{+0.5}_{-0.5} - 2.31^{+0.9}_{-0.9}$
J1952 + 3252	9.09×10^{-26}	$(1.0 \pm 0.7) \times 10^{-4}$	25.2	0.9 ± 0.6	0.8	$0.5^{+0.4}_{-0.4} - 1.1^{+0.8}_{-0.8}$
J2022 + 3842	1.32×10^{-25}	$(7.4 \pm 1.5) \times 10^{-4}$	184.0	1.2 ± 0.3	1.4	$0.7^{+0.2}_{-0.2} - 1.5^{+0.3}_{-0.3}$
J2043 + 2740	1.12×10^{-24}	$(3.6 \pm 1.4) \times 10^{-3}$	⋯	17.8 ± 7.0	⋯	$10.3^{+4.0}_{-4.0} - 21.42^{+9.0}_{-9.0}$
J2124 − 3358	5.97×10^{-26}	$(1.3 \pm 0.3) \times 10^{-7}$	⋯	14.0 ± 3.3	⋯	$7.3^{+1.8}_{-1.8} - 17.4^{+4.2}_{-4.2}$
J2229 + 6114	1.39×10^{-25}	$(2.7 \pm 1.8) \times 10^{-4}$	65.8	0.4 ± 0.3	0.2	$0.3^{+0.2}_{-0.2} - 0.5^{+0.4}_{-0.4}$

and are of the order of 5.5×10^{-26} which, however, are above the spin-down limit. The lowest ellipticity UL has been set for J1300 + 1240, of about 3.3×10^{-7}. We have been able to surpass the spin-down limit for the pulsars J0205 + 6449, J0534 + 2200 (Crab), J0835 − 4510 (Vela), J1400 − 6325, J1813 − 1246 (assuming the lower bound for the distance), J1813 − 1749, J1833 − 1034, and J2229 + 6114. For J0940 − 5428, while the median value

of the UL is below the spin-down limit, a small fraction of the individual results are above. For J1747 − 2809 and J1952 + 3252, we are close to surpassing the spin-down limit[4]; see Table IV. For all the pulsars for which we have surpassed the spin-down limit, we have computed the upper limit on the ratio of the GW to the rotational energy loss. The lower ULs on the GW energy loss are for J0534 + 2200 and J1400 − 6325 corresponding to a fraction of about 0.8%. The lowest ULs on the GW amplitude and ellipticity among the pulsars for which we have surpassed the spin-down limit are, respectively, 8.29×10^{-26} and 1.78×10^{-5} for J1400 − 6325. For a canonical pulsar with a radius of about 10 km, this number would correspond to a maximum surface deformation of about 5 cm.

For the remaining 22 targets, we were not able to surpass the spin-down limit. Table IV roughly suggests to us that an improvement in sensitivity of a factor 3 is needed for most of the low-frequency pulsars. It must be considered, however, that the spin-down limits have been computed assuming a canonical value for the moment of inertia of 10^{38} kg m^2. In fact, it could be significantly larger, depending on the NS equation of state, up to $\sim 3 \times 10^{38}$ kg m^2, implying a spin-down limit $\sim\sqrt{(3)}$ times larger.

VI. CONCLUSION

Overall, the narrow-band search over O2 data has brought an improvement with respect to previous searches in terms of ULs. On the other hand, ULs are similar to those found in O1 for pulsars with rotation frequency below 30 Hz. For instance, the UL on the Vela Pulsar (around 22 Hz) has improved by 10%, while the UL on J0205 + 6449[5] has improved by about 22%. On the other hand, for pulsars with expected GW frequencies >30 Hz, the UL is improved even by a factor 2. The UL on J0534 + 2200 did not improve, since in O2 we split the analysis in two different chunks due to the presence of the glitch. For this reason, the UL both before and after the glitch is comparable to the one found in the O1 analysis. We have also been able to surpass the spin-down limit for two pulsars that were not analyzed in O1, J0940 − 5428, J1747 − 2809.

We still have not been able to surpass the spin-down limit for the millisecond pulsars and for low-frequency pulsars with spin-down below $\sim 10^{-12}$ Hz/s. However, we have been able to surpass the spin-down limit for low-frequency and high energetic pulsars (such as Crab or J1833 − 1034) or for low-frequency pulsars that are close to Earth.

[4]Excluding a frequency band heavily contaminated by noise.

[5]Please note that the spin-down limit of this pulsar has been computed using two different distances in O1 and O2. For O1, we used 2.0 kpc [54], while for O2 the nominal ephemeris value was 3.2 kpc.

ACKNOWLEDGMENTS

The authors gratefully acknowledge the support of the United States National Science Foundation (NSF) for the construction and operation of the LIGO Laboratory and Advanced LIGO as well as the Science and Technology Facilities Council (STFC) of the United Kingdom, the Max-Planck-Society (MPS), and the State of Niedersachsen/Germany for support of the construction of Advanced LIGO and construction and operation of the GEO600 detector. Additional support for Advanced LIGO was provided by the Australian Research Council. The authors gratefully acknowledge the Italian Istituto Nazionale di Fisica Nucleare (INFN), the French Centre National de la Recherche Scientifique (CNRS), and the Foundation for Fundamental Research on Matter supported by the Netherlands Organisation for Scientific Research for the construction and operation of the Virgo detector and the creation and support of the European Gravitational Observatory consortium. The authors also gratefully acknowledge research support from these agencies as well as by the Council of Scientific and Industrial Research of India, the Department of Science and Technology, India, the Science & Engineering Research Board, India, the Ministry of Human Resource Development, India, the Spanish Agencia Estatal de Investigación, the Vicepresidència i Conselleria d'Innovació, Recerca i Turisme and the Conselleria d'Educació i Universitat del Govern de les Illes Balears, the Conselleria d'Educació, Investigació, Cultura i Esport de la Generalitat Valenciana, the National Science Centre of Poland, the Swiss National Science Foundation, the Russian Foundation for Basic Research, the Russian Science Foundation, the European Commission, the European Regional Development Funds, the Royal Society, the Scottish Funding Council, the Scottish Universities Physics Alliance, the Hungarian Scientific Research Fund, the Lyon Institute of Origins, the National Research, Development and Innovation Office Hungary, the National Research Foundation of Korea, Industry Canada and the Province of Ontario through the Ministry of Economic Development and Innovation, the Natural Science and Engineering Research Council Canada, the Canadian Institute for Advanced Research, the Brazilian Ministry of Science, Technology, Innovations, and Communications, the International Center for Theoretical Physics South American Institute for Fundamental Research, the Research Grants Council of Hong Kong, the National Natural Science Foundation of China, the Leverhulme Trust, the Research Corporation, the Ministry of Science and Technology, Taiwan, and the Kavli Foundation. The authors gratefully acknowledge the support of the NSF, STFC, MPS, INFN, CNRS, and the State of Niedersachsen/Germany for provision of computational resources. Work at Naval Research Laboratory is supported by the National Aeronautics and Space Administration. The authors acknowledge the anonymous referees for helping improve this paper. This work has been assigned LIGO Document No. LIGO-P1800391.

TABLE V. Accuracy of the parameter estimation for the O2 hardware injections. The first three columns report the name, frequency, and spin-down of the hardware injections (reference time of December 1, 2017 UTC 00:00:00). The last three columns report the relative errors in percentage for the parameter estimation. The relative errors are defined in the text.

Name	$f_{\rm gw}$ (Hz)	$\dot{f}_{\rm gw}$ (Hz/s)	ϵ_{h_0}	ϵ_η	ϵ_ψ
Pulsar 2	575.16	-1.37×10^{-13}	6%	0.3%	...
Pulsar 3	108.86	-1.46×10^{-17}	0.01%	0.3%	2%
Pulsar 5	52.81	-4.03×10^{-18}	3%	0.07%	1%
Pulsar 8	190.46	-8.65×10^{-9}	8%	0.03%	0.07%

APPENDIX A: VALIDATION WITH HARDWARE INJECTIONS

Hardware injections are simulated signals in LIGO-Virgo data for testing purposes. These artificial signals are injected by a control system which acts on the mirror and simulates a CW signal. The hardware injections are continuously monitored and their injected parameters are known. In order to validate the efficiency of the pipeline used in this paper, we have looked for four hardware injections in LIGO data studying the accuracy of the recovered parameters. We define the relative error on the CW amplitude recovery as $\epsilon_{h_0} = 1 - h_0^{\rm esti}/h_0^{\rm inj}$, where $h_0^{\rm inj}$ is the injected CW amplitude and $h_0^{\rm esti}$ is the recovered value, whereas we define the relative error on the angular parameters ψ, η as $\epsilon_\psi = |\psi^{\rm inj} - \psi^{\rm esti}|/90$ deg and $\epsilon_\eta = |\eta^{\rm inj} - \eta^{\rm esti}|/2$. Table V reports the errors on the parameter estimation for the validation tests performed with the O2 hardware injections.

APPENDIX B: VALIDATION OF THE THRESHOLD

The narrow-band search is based on the five-vector method [29] that was implemented originally for *targeted searches*. In that context, just one template is explored for each detector, and an overall threshold on the p value of, say, 1% for the candidate selection, is sufficient to efficiently recover 95% of injected signals with SNR = 8. However, in narrow-band searches, we are exploring a large number of templates in a frequency region of about 0.04 Hz or more, using two detectors that have different data quality, i.e., different level of noise and duty cycle. The threshold in this case is computed by using as noise background the values of the statistic excluded from the local maxima selection and then extrapolating the long tails of the distribution. By definition, these excluded points are representative of the noise level in the given frequency bands. This means that, if the noise level in the 10^{-4} Hz wide frequency subband that we are analyzing is slightly higher than the noise level in the overall frequency region from which we are generating noise backgrounds, then close-to-threshold outliers will occur. These close-to-threshold outliers may not be completely distinguishable from the actual noise. As an example, we have generated 200 software injections with amplitude h_0 fixed to the one that generated a 1% p-value outlier in the postglitch analysis of pulsar J0534 + 2200. We have estimated the recovered signal-to-noise ratio of the injections by integrating coherently more and more data from LHO and LLO. If the injections are distinguishable from the noise, we expect 95% of the injections to have a recovered signal-to-noise ratio greater than 8. However, it is shown by Fig. 2 that this is not the case. For a full coherent LHO-LLO search, the distribution of the recovered SNR is below 8. We have also performed the same test by injecting fake signals with an amplitude h_0 that would correspond to a 0.1% outlier. In this case, as shown in Fig. 2, the recovered SNR of the injections is higher than 8, confirming that the 0.1% p-value threshold represents a more conservative choice while recovering CW signals.

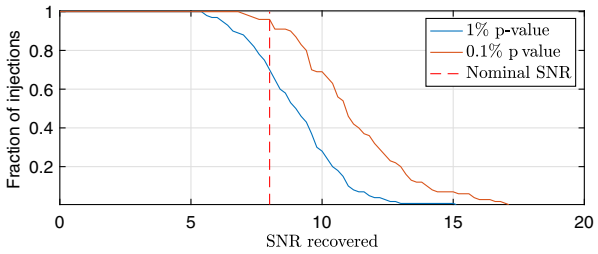

FIG. 2. Vertical axis: Fraction of injections recovered with a SNR equal to or higher than the one indicated on the *horizontal axis*. The different line colors indicate a set of software injections that would produce an outlier at 1% and 0.1% according to the evaluation of the noise-only distribution of the detection statistic. The red dashed vertical line indicates the SNR = 8 threshold that is commonly used to distinguish the signal from the noise.

APPENDIX C: FOLLOW-UP TEST CASES

We report in this Appendix some explanatory plots of the analysis steps used for outliers follow-up. The first step

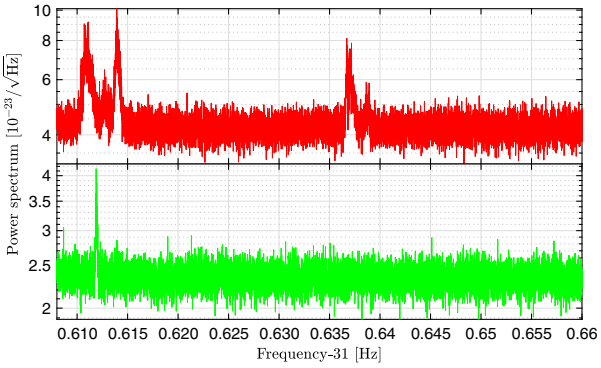

FIG. 3. Top: LHO spectrum around the expected frequency of J1105 − 6107. Bottom: LLO spectrum around the expected signal frequency of J1105 − 6107. In both detectors, we see the contribution of various noise lines which are known combs with fundamental frequency 0.987925 Hz in LLO and 2.109223 Hz in LHO.

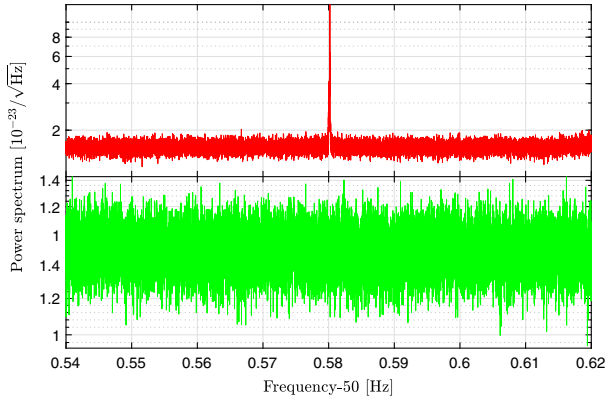

FIG. 4. Top: LHO spectrum around the expected frequency of J1952 + 3252. Bottom: LLO spectrum around the expected frequency of J1952 + 3252. In LHO we see the contribution of various noise lines due to combs with fundamental frequencies 2.109223, 1.9455045, and 1.945437 Hz in LHO.

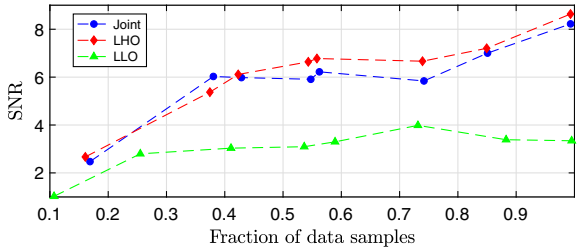

FIG. 5. Example of the first stage follow-up for one of the candidates of J1105 + 6107 that were not vetoed. The recovered SNR of the outlier is on the vertical axis, while the horizontal axis indicates the fraction of data samples that we are integrating with the matched filter. The outlier is visible only in LHO and propagates to the joint analysis.

consisted of checking if a known noise line was present in the proximity of the outlier. We considered an outlier consistent with a known noise disturbance if it was found in a frequency region covered by the frequency variation of the noise line due to the Doppler and spin-down corrections.

Many of the outliers found in the case of the pulsar J1105 − 6107 and J1952 + 3252 originated from vetoed combs in one or both of the detectors. Figures 3 and 4 show the spectra of the time series obtained for the J1105 − 6107 and J1952 + 3252 outliers. In the first case, noise combs pollute both LLO and LHO, while in the second case, different noise combs contribute to the same noise disturbance at 50.58 Hz in the LHO data.

The second step of the follow-up chain was to study the evolution of the recovered CW amplitude h_0 and the recovered SNR of the outlier with respect to the integration time. In Fig. 5, we report the recovered SNR for different integration times. In this frequency region, the LHO noise floor is about 2 times higher than the LLO noise floor. Hence, in the presence of a reliable CW outlier, we would expect the recovered SNR to be higher in LLO and the joint analysis. As shown in Fig. 5, this is not the case, and the outlier is probably due to an unknown noise disturbance in LHO.

The last step of the follow-up consisted of studying the noise properties with software injections around the candidates. The software injections had amplitude h_0 equal to the one recovered from the most sensitive search. This corresponds to LLO for most of the frequencies <40 Hz, while it is the joint search if the noise floor of the two detectors is comparable. The recovered distribution of the CW amplitude and SNR for the software injections is then plotted with respect to the integration time of the analysis and compared with the recovered CW amplitude and SNR for the outlier. Figure 6 shows the distributions of the recovered SNR and CW amplitude for 200 software injections with an amplitude fixed at $h_0 = 3.9 \times 10^{-26}$, which is the one recovered for the outlier of the millisecond pulsar J1300 + 1240 in the joint search. The software injections have a frequency at least 10^{-3} Hz away from the actual outlier, in such a way as to not interfere with the

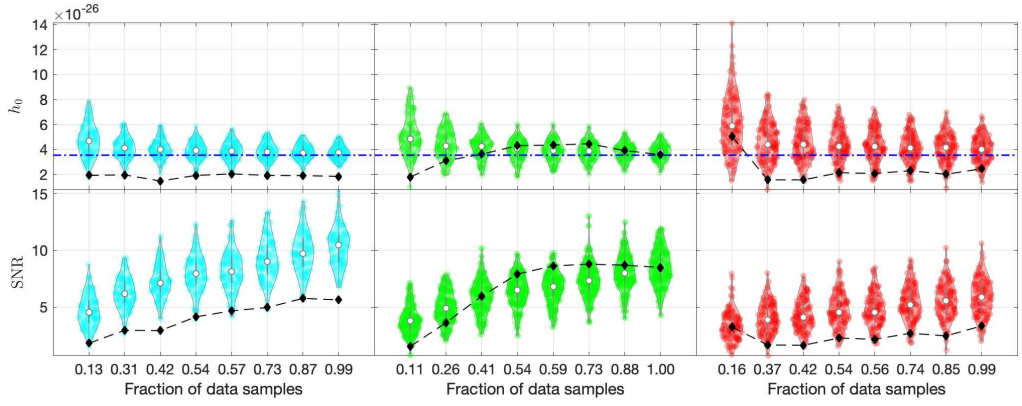

FIG. 6. These plots show the distribution of the recovered CW amplitude h_0 and SNR for 200 software injections in the frequency region around the outlier of the millisecond pulsar J1300 + 1240. The black dashed line indicates the observed estimator for the outlier. First and second rows of plots: Recovered CW amplitude and SNR. First, second, and third columns of plots: Joint, LLO, and LHO searches.

outlier. From Fig. 6 we can see that the outlier seems to be compatible with the results of the software injections in LLO data, but on the other hand, it is not compatible with the joint and LHO analysis. In this frequency region, the detector's noise floor is similar, and we would expect comparable results for the LLO and LHO analysis. The software injections show that a signal with amplitude $h_0 \approx 3.9 \times 10^{-26}$ would be distinguishable from the noise in the joint search because the recovered SNR of the software injections with the same amplitude for a joint fully coherent search is always higher than 7.5. On the contrary, in the joint search the SNR of the actual outlier (black dashed line) is low and not compatible with the results of the software injections, suggesting that the outlier is due to an unknown noise disturbance present in LLO.

[1] J. Aasi *et al.* (LIGO Scientific Collaboration), Advanced LIGO, Classical Quantum Gravity **32**, 115012 (2015).

[2] B. P. Abbott *et al.* (LIGO Scientific and Virgo Collaborations), GW150914: The Advanced LIGO Detectors in the Era of First Discoveries., Phys. Rev. Lett. **116**, 131103 (2016).

[3] F. a Acernese *et al.* (Virgo Collaboration), Advanced Virgo: A second-generation interferometric gravitational wave detector, Classical Quantum Gravity **32**, 024001 (2015).

[4] B. P. Abbott *et al.* (LIGO Scientific and Virgo Collaborations), GWTC-1: A gravitational-wave transient catalog of compact binary mergers observed by LIGO and Virgo during the first and second observing runs, arXiv:1811.12907.

[5] B. P. Abbott *et al.* (LIGO Scientific and Virgo Collaborations), Observation of Gravitational Waves from a Binary Black Hole Merger, Phys. Rev. Lett. **116**, 1 (2016).

[6] B. P. Abbott *et al.* (LIGO Scientific and Virgo Collaborations), GW151226: Observation of Gravitational Waves from a 22-Solar-Mass Binary Black Hole Coalescence, Phys. Rev. Lett. **116**, 241103 (2016).

[7] B. P. Abbott *et al.* (LIGO Scientific and Virgo Collaborations), GW170814: A Three-Detector Observation of Gravitational Waves from a Binary Black Hole Coalescence, Phys. Rev. Lett. **119**, 141101 (2017).

[8] B. P. Abbott *et al.* (LIGO Scientific and Virgo Collaborations), GW170104: Observation of a 50-Solar-Mass Binary Black Hole Coalescence at Redshift 0.2, Phys. Rev. Lett. **118**, 221101 (2017).

[9] B. P. Abbott *et al.* (LIGO Scientific and Virgo Collaborations), GW170608: Observation of a 19-solar-mass binary black hole coalescence, Astrophys. J. Lett. **851**, L35 (2017).

[10] B. P. Abbott *et al.* (LIGO Scientific and Virgo Collaborations), GW170817: Observation of Gravitational Waves from a Binary Neutron Star Inspiral, Phys. Rev. Lett. **119**, 161101 (2017).

[11] B. P. Abbott *et al.* (LIGO Scientific Collaboration), Setting upper limits on the strength of periodic gravitational waves from PSR J1939 + 2134 using the first science data from the GEO 600 and LIGO detectors, Phys. Rev. D **69**, 082004 (2004).

[12] B. P. Abbott *et al.* (LIGO Scientific Collaboration), Limits on Gravitational-Wave Emission from Selected Pulsars Using LIGO Data, Phys. Rev. Lett. **94**, 181103 (2005).

[13] B. P. Abbott *et al.* (LIGO Scientific and Virgo Collaborations), Upper limits on gravitational wave emission from 78 radio pulsars, Phys. Rev. D **76**, 042001 (2007).

[14] B. P. Abbott *et al.* (LIGO Scientific and Virgo Collaborations), Beating the spin-down limit on gravitational wave emission from the Crab Pulsar, Astrophys. J. Lett. **683**, L45 (2008).

[15] B. P. Abbott *et al.* (LIGO Scientific and Virgo Collaborations), Searches for gravitational waves from known pulsars with science run 5 LIGO data, Astrophys. J. **713**, 671 (2010).

[16] J. Abadie *et al.* (LIGO Scientific and Virgo Collaborations), Beating the spin-down limit on gravitational wave emission from the Vela Pulsar, Astrophys. J. **737**, 93 (2011).

[17] J. Aasi *et al.* (LIGO Scientific and Virgo Collaborations), Gravitational waves from known pulsars: Results from the initial detector era, Astrophys. J. **785**, 119 (2014).

[18] B. P. Abbott *et al.* (LIGO Scientific and Virgo Collaborations), First search for gravitational waves from known pulsars with Advanced LIGO, Astrophys. J. **839**, 12 (2017).

[19] B. P. Abbott *et al.* (LIGO Scientific and Virgo Collaborations), Searches for gravitational waves from known pulsars at two harmonics in 2015–2017 LIGO data, arXiv:1902.08507.

[20] J. Aasi *et al.* (LIGO Scientific and Virgo Collaborations), Searches for continuous gravitational waves from nine young supernova remnants, Astrophys. J. **813**, 39 (2015).

[21] B. P. Abbott *et al.* (LIGO Scientific and Virgo Collaborations), Searches for continuous gravitational waves from fifteen supernova remnants and Fomalhaut b with Advanced LIGO, Astrophys. J. Lett. **875**, 122 (2019).

[22] J. Aasi *et al.* (LIGO Scientific and Virgo Collaborations), Directed search for gravitational waves from Scorpius X-1 with initial LIGO data, Phys. Rev. D **91**, 062008 (2015).

[23] B. P. Abbott *et al.* (LIGO Scientific and Virgo Collaborations), Search for gravitational waves from Scorpius X-1 in the first Advanced LIGO observing run with a hidden Markov model, Phys. Rev. D **95**, 122003 (2017).

[24] B. P. Abbott *et al.* (LIGO Scientific and Virgo Collaborations), Upper limits on gravitational waves from Scorpius X-1 from a model-based cross-correlation search in Advanced LIGO data, Astrophys. J. **847**, 47 (2017).

[25] B. P. Abbott *et al.* (LIGO Scientific and Virgo Collaborations), First Search for Nontensorial Gravitational Waves from Known Pulsars, Phys. Rev. Lett. **120**, 031104 (2018).

[26] J. Aasi *et al.* (LIGO Scientific and Virgo Collaborations), Narrow-band search of continuous gravitational-wave signals from Crab and Vela Pulsars in Virgo VSR4 data, Phys. Rev. D **91**, 022004 (2015).
[27] B. P. Abbott *et al.* (LIGO Scientific and Virgo Collaborations), First narrow-band search for continuous gravitational waves from known pulsars in advanced detector data, Phys. Rev. D **96**, 122006 (2017).
[28] D. I. Jones and N. Andersson, Gravitational waves from freely precessing neutron stars, Mon. Not. R. Astron. Soc. **331**, 203 (2002).
[29] P. Astone, S. D'Antonio, S. Frasca, and C. Palomba, A method for detection of known sources of continuous gravitational wave signals in non-stationary data, Classical Quantum Gravity **27**, 194016 (2010).
[30] P. Jaranowski, A. Królak, and B. F. Schutz, Data analysis of gravitational-wave signals from spinning neutron stars: The signal and its detection, Phys. Rev. D **58**, 063001 (1998).
[31] M. Bejger, Parameters of rotating neutron stars with and without hyperons, Astron. Astrophys. **552**, A59 (2013).
[32] P. Astone, A. Colla, S. D'Antonio, S. Frasca, C. Palomba, and R. Serafinelli, Method for narrow-band search of continuous gravitational wave signals, Phys. Rev. D **89**, 062008 (2014).
[33] S. Mastrogiovanni, P. Astone, S. D'Antonio, S. Frasca, G. Intini, P. Leaci, A. Miller, C. Palomba, O. J. Piccinni, and A. Singhal, An improved algorithm for narrow-band searches of continuous gravitational waves, Classical Quantum Gravity **34**, 135007 (2017).
[34] C. Cahillane, J. Betzwieser, D. A. Brown, E. Goetz, E. D. Hall, K. Izumi, S. Kandhasamy, S. Karki, J. S. Kissel, G. Mendell, R. L. Savage, D. Tuyenbayev, A. Urban, A. Viets, M. Wade, and A. J. Weinstein, Calibration uncertainty for Advanced LIGO's first and second observing runs, Phys. Rev. D **96**, 102001 (2017).
[35] R. N. Manchester, G. B. Hobbs, A. Teoh, and M. Hobbs, The Australia Telescope National Facility Pulsar Catalogue, Astron. J. **129**, 1993 (2005).
[36] J. M. Yao, R. N. Manchester, and N. Wang, A new electron-density model for estimation of pulsar and FRB distances, Astrophys. J. **835**, 29 (2017).
[37] R. Kothes, Distance and age of the pulsar wind nebula 3C 58, Astron. Astrophys. **560**, A18 (2013).
[38] D. L. Kaplan, S. Chatterjee, B. M. Gaensler, and J. Anderson, A precise proper motion for the Crab Pulsar, and the difficulty of testing spin-kick alignment for young neutron stars, Astrophys. J. **677**, 1201 (2008).
[39] G. Pietrzyński *et al.*, An eclipsing-binary distance to the Large Magellanic Cloud accurate to two percent, Nature (London) **495**, 76 (2013).
[40] R. Dodson, D. Legge, J. E. Reynolds, and P. M. McCulloch, The Vela Pulsar's proper motion and parallax derived from VLBI observations, Astrophys. J. **596**, 1137 (2003).
[41] J. P. W. Verbiest, J. M. Weisberg, A. A. Chael, K. J. Lee, and D. R. Lorimer, On pulsar distance measurements and their uncertainties, Astrophys. J. **755**, 39 (2012).
[42] M. Renaud, V. Marandon, E. V. Gotthelf, J. Rodriguez, R. Terrier, F. Mattana, F. Lebrun, J. A. Tomsick, and R. N. Manchester, Discovery of a highly energetic pulsar associated with IGR J14003 − 6326 in the young uncataloged galactic supernova remnant G310.6-1.6, Astrophys. J. **716**, 663 (2010).
[43] M. Marelli, A. Harding, D. Pizzocaro, A. De Luca, K. S. Wood, P. Caraveo, D. Salvetti, P. M. Saz Parkinson, and F. Acero, On the puzzling high-energy pulsations of the energetic radio-quiet γ-ray pulsar J1813 − 1246, Astrophys. J. **795**, 168 (2014).
[44] J. P. Halpern, E. V. Gotthelf, and F. Camilo, Spin-down measurement of PSR J1813 − 1749: The energetic pulsar powering HESS J1813 − 178, Astrophys. J. Lett. **753**, L14 (2012).
[45] F. Camilo, S. M. Ransom, B. M. Gaensler, P. O. Slane, D. R. Lorimer, J. Reynolds, R. N. Manchester, and S. S. Murray, PSR J1833 − 1034: Discovery of the central young pulsar in the supernova remnant G21.5-0.9, Astrophys. J. **637**, 456 (2006).
[46] E. V. Gotthelf and J. P. Halpern, Discovery of a young, energetic 70.5 ms pulsar associated with the TeV gamma-ray source HESS J1837 − 069, Astrophys. J. **681**, 515 (2008).
[47] P. Arumugasamy, G. G. Pavlov, and O. Kargaltsev, XMM-Newton observations of young and energetic pulsar J2022 + 3842, Astrophys. J. **790**, 103 (2014).
[48] G. Desvignes *et al.*, High-precision timing of 42 millisecond pulsars with the European Pulsar Timing Array, Mon. Not. R. Astron. Soc. **458**, 3341 (2016).
[49] J. P. Halpern, F. Camilo, E. V. Gotthelf, D. J. Helfand, M. Kramer, A. G. Lyne, K. M. Leighly, and M. Eracleous, PSR J2229 + 6114: Discovery of an energetic young pulsar in the error box of the EGRET source 3EG J2227 + 6122, Astrophys. J. Lett. **552**, L125 (2001).
[50] P. Leaci and R. Prix, Directed searches for continuous gravitational waves from binary systems: Parameter-space metrics and optimal Scorpius X-1 sensitivity, Phys. Rev. D **91**, 102003 (2015).
[51] J. Palfreyman, J. M. Dickey, A. Hotan, S. Ellingsen, and W. van Straten, Alteration of the magnetosphere of the Vela Pulsar during a glitch, Nature (London) **556**, 219 (2018).
[52] P. B. Covas, A. Effler, E. Goetz, P. M. Meyers, A. Neunzert, M. Oliver, B. L. Pearlstone, V. J. Roma, R. M. S. Schofield, V. B. Adya *et al.*, Identification and mitigation of narrow spectral artifacts that degrade searches for persistent gravitational waves in the first two observing runs of Advanced LIGO, Phys. Rev. D **97**, 082002 (2018).
[53] N. K. Johnson-McDaniel, Gravitational wave constraints on the shape of neutron stars, Phys. Rev. D **88**, 044016 (2013).
[54] R. Kothes, Distance and age of the pulsar wind nebula 3C 58, Astron. Astrophys. **560**, A18 (2013).

B. P. Abbott,[1] R. Abbott,[1] T. D. Abbott,[2] S. Abraham,[3] F. Acernese,[4,5] K. Ackley,[6] C. Adams,[7] R. X. Adhikari,[1] V. B. Adya,[8,9] C. Affeldt,[8,9] M. Agathos,[10] K. Agatsuma,[11] N. Aggarwal,[12] O. D. Aguiar,[13] L. Aiello,[14,15] A. Ain,[3] P. Ajith,[16] G. Allen,[17] A. Allocca,[18,19] M. A. Aloy,[20] P. A. Altin,[21] A. Amato,[22] A. Ananyeva,[1] S. B. Anderson,[1] W. G. Anderson,[23] S. V. Angelova,[24] S. Antier,[25] S. Appert,[1] K. Arai,[1] M. C. Araya,[1] J. S. Areeda,[26] M. Arène,[27] N. Arnaud,[25,28] S. Ascenzi,[29,30] G. Ashton,[6] S. M. Aston,[7] P. Astone,[31] F. Aubin,[32] P. Aufmuth,[9] K. AultONeal,[33] C. Austin,[2] V. Avendano,[34] A. Avila-Alvarez,[26] S. Babak,[35,27] P. Bacon,[27] F. Badaracco,[14,15] M. K. M. Bader,[36] S. Bae,[37] P. T. Baker,[38] F. Baldaccini,[39,40] G. Ballardin,[28] S. W. Ballmer,[41] S. Banagiri,[42] J. C. Barayoga,[1] S. E. Barclay,[43] B. C. Barish,[1] D. Barker,[44] K. Barkett,[45] S. Barnum,[12] F. Barone,[4,5] B. Barr,[43] L. Barsotti,[12] M. Barsuglia,[27] D. Barta,[46] J. Bartlett,[44] I. Bartos,[47] R. Bassiri,[48] A. Basti,[18,19] M. Bawaj,[49,40] J. C. Bayley,[43] M. Bazzan,[50,51] B. Bécsy,[52] M. Bejger,[27,53] I. Belahcene,[25] A. S. Bell,[43] D. Beniwal,[54] B. K. Berger,[48] G. Bergmann,[8,9] S. Bernuzzi,[55,56] J. J. Bero,[57] C. P. L. Berry,[58] D. Bersanetti,[59] A. Bertolini,[36] J. Betzwieser,[7] R. Bhandare,[60] J. Bidler,[26] I. A. Bilenko,[61] S. A. Bilgili,[38] G. Billingsley,[1] J. Birch,[7] R. Birney,[24] O. Birnholtz,[57] S. Biscans,[1,12] S. Biscoveanu,[6] A. Bisht,[9] M. Bitossi,[28,19] M. A. Bizouard,[25] J. K. Blackburn,[1] C. D. Blair,[7] D. G. Blair,[62] R. M. Blair,[44] S. Bloemen,[63] N. Bode,[8,9] M. Boer,[64] Y. Boetzel,[65] G. Bogaert,[64] F. Bondu,[66] E. Bonilla,[48] R. Bonnand,[32] P. Booker,[8,9] B. A. Boom,[36] C. D. Booth,[67] R. Bork,[1] V. Boschi,[28] S. Bose,[68,3] K. Bossie,[7] V. Bossilkov,[62] J. Bosveld,[62] Y. Bouffanais,[27] A. Bozzi,[28] C. Bradaschia,[19] P. R. Brady,[23] A. Bramley,[7] M. Branchesi,[14,15] J. E. Brau,[69] T. Briant,[70] J. H. Briggs,[43] F. Brighenti,[71,72] A. Brillet,[64] M. Brinkmann,[8,9] V. Brisson,[25,†] P. Brockill,[23] A. F. Brooks,[1] D. D. Brown,[54] S. Brunett,[1] A. Buikema,[12] T. Bulik,[73] H. J. Bulten,[74,36] A. Buonanno,[35,75] D. Buskulic,[32] C. Buy,[27] R. L. Byer,[48] M. Cabero,[8,9] L. Cadonati,[76] G. Cagnoli,[22,77] C. Cahillane,[1] J. Calderón Bustillo,[6] T. A. Callister,[1] E. Calloni,[78,5] J. B. Camp,[79] W. A. Campbell,[6] M. Canepa,[80,59] K. C. Cannon,[81] H. Cao,[54] J. Cao,[82] E. Capocasa,[27] F. Carbognani,[28] S. Caride,[83] M. F. Carney,[58] G. Carullo,[18] J. Casanueva Diaz,[19] C. Casentini,[29,30] S. Caudill,[36] M. Cavaglià,[84] F. Cavalier,[25] R. Cavalieri,[28] G. Cella,[19] P. Cerdá-Durán,[20] G. Cerretani,[18,19] E. Cesarini,[85,30] O. Chaibi,[64] K. Chakravarti,[3] S. J. Chamberlin,[86] M. Chan,[43] S. Chao,[87] P. Charlton,[88] E. A. Chase,[58] E. Chassande-Mottin,[27] D. Chatterjee,[23] M. Chaturvedi,[60] B. D. Cheeseboro,[38] H. Y. Chen,[89] X. Chen,[62] Y. Chen,[45] H.-P. Cheng,[47] C. K. Cheong,[90] H. Y. Chia,[47] A. Chincarini,[59] A. Chiummo,[28] G. Cho,[91] H. S. Cho,[92] M. Cho,[75] N. Christensen,[64,93] Q. Chu,[62] S. Chua,[70] K. W. Chung,[90] S. Chung,[62] G. Ciani,[50,51] A. A. Ciobanu,[54] R. Ciolfi,[94,95] F. Cipriano,[64] A. Cirone,[80,59] F. Clara,[44] J. A. Clark,[76] P. Clearwater,[96] F. Cleva,[64] C. Cocchieri,[84] E. Coccia,[14,15] P.-F. Cohadon,[70] D. Cohen,[25] R. Colgan,[97] M. Colleoni,[98] C. G. Collette,[99] C. Collins,[11] L. R. Cominsky,[100] M. Constancio Jr.,[13] L. Conti,[51] S. J. Cooper,[11] P. Corban,[7] T. R. Corbitt,[2] I. Cordero-Carrión,[101] K. R. Corley,[97] N. Cornish,[52] A. Corsi,[83] S. Cortese,[28] C. A. Costa,[13] R. Cotesta,[35] M. W. Coughlin,[1] S. B. Coughlin,[67,58] J.-P. Coulon,[64] S. T. Countryman,[97] P. Couvares,[1] P. B. Covas,[98] E. E. Cowan,[76] D. M. Coward,[62] M. J. Cowart,[7] D. C. Coyne,[1] R. Coyne,[102] J. D. E. Creighton,[23] T. D. Creighton,[103] J. Cripe,[2] M. Croquette,[70] S. G. Crowder,[104] T. J. Cullen,[2] A. Cumming,[43] L. Cunningham,[43] E. Cuoco,[28] T. Dal Canton,[79] G. Dálya,[105] S. L. Danilishin,[8,9] S. D'Antonio,[30] K. Danzmann,[9,8] A. Dasgupta,[106] C. F. Da Silva Costa,[47] L. E. H. Datrier,[43] V. Dattilo,[28] I. Dave,[60] M. Davier,[25] D. Davis,[41] E. J. Daw,[107] D. DeBra,[48] M. Deenadayalan,[3] J. Degallaix,[22] M. De Laurentis,[78,5] S. Deléglise,[70] W. Del Pozzo,[18,19] L. M. DeMarchi,[58] N. Demos,[12] T. Dent,[8,9,108] R. De Pietri,[109,56] J. Derby,[26] R. De Rosa,[78,5] C. De Rossi,[22,28] R. DeSalvo,[110] O. de Varona,[8,9] S. Dhurandhar,[3] M. C. Díaz,[103] T. Dietrich,[36] L. Di Fiore,[5] M. Di Giovanni,[111,95] T. Di Girolamo,[78,5] A. Di Lieto,[18,19] B. Ding,[99] S. Di Pace,[112,31] I. Di Palma,[112,31] F. Di Renzo,[18,19] A. Dmitriev,[11] Z. Doctor,[89] F. Donovan,[12] K. L. Dooley,[67,84] S. Doravari,[8,9] I. Dorrington,[67] T. P. Downes,[23] M. Drago,[14,15] J. C. Driggers,[44] Z. Du,[82] J.-G. Ducoin,[25] P. Dupej,[43] S. E. Dwyer,[44] P. J. Easter,[6] T. B. Edo,[107] M. C. Edwards,[93] A. Effler,[7] P. Ehrens,[1] J. Eichholz,[1] S. S. Eikenberry,[47] M. Eisenmann,[32] R. A. Eisenstein,[12] R. C. Essick,[89] H. Estelles,[98] D. Estevez,[32] Z. B. Etienne,[38] T. Etzel,[1] M. Evans,[12] T. M. Evans,[7] V. Fafone,[29,30,14] H. Fair,[41] S. Fairhurst,[67] X. Fan,[82] S. Farinon,[59] B. Farr,[69] W. M. Farr,[11] E. J. Fauchon-Jones,[67] M. Favata,[34] M. Fays,[107] M. Fazio,[113] C. Fee,[114] J. Feicht,[1] M. M. Fejer,[48] F. Feng,[27] A. Fernandez-Galiana,[12] I. Ferrante,[18,19] E. C. Ferreira,[13] T. A. Ferreira,[13] F. Ferrini,[28] F. Fidecaro,[18,19] I. Fiori,[28] D. Fiorucci,[27] M. Fishbach,[89] R. P. Fisher,[41,115] J. M. Fishner,[12] M. Fitz-Axen,[42] R. Flaminio,[32,116] M. Fletcher,[43] E. Flynn,[26] H. Fong,[117] J. A. Font,[20,118] P. W. F. Forsyth,[21] J.-D. Fournier,[64] S. Frasca,[112,31] F. Frasconi,[19] Z. Frei,[105] A. Freise,[11] R. Frey,[69] V. Frey,[25] P. Fritschel,[12] V. V. Frolov,[7] P. Fulda,[47] M. Fyffe,[7] H. A. Gabbard,[43] B. U. Gadre,[3] S. M. Gaebel,[11] J. R. Gair,[119] L. Gammaitoni,[39] M. R. Ganija,[54] S. G. Gaonkar,[3] A. Garcia,[26] C. García-Quirós,[98] F. Garufi,[78,5] B. Gateley,[44] S. Gaudio,[33] G. Gaur,[120] V. Gayathri,[121] G. Gemme,[59] E. Genin,[28] A. Gennai,[19] D. George,[17] J. George,[60] L. Gergely,[122] V. Germain,[32] S. Ghonge,[76] Abhirup Ghosh,[16] Archisman Ghosh,[36] S. Ghosh,[23] B. Giacomazzo,[111,95] J. A. Giaime,[2,7] K. D. Giardina,[7] A. Giazotto,[19,†] K. Gill,[33] G. Giordano,[4,5] L. Glover,[110] P. Godwin,[86] E. Goetz,[44] R. Goetz,[47]

B. Goncharov,[6] G. González,[2] J. M. Gonzalez Castro,[18,19] A. Gopakumar,[123] M. L. Gorodetsky,[61] S. E. Gossan,[1] M. Gosselin,[28] R. Gouaty,[32] A. Grado,[124,5] C. Graef,[43] M. Granata,[22] A. Grant,[43] S. Gras,[12] P. Grassia,[1] C. Gray,[44] R. Gray,[43] G. Greco,[71,72] A. C. Green,[11,47] R. Green,[67] E. M. Gretarsson,[33] P. Groot,[63] H. Grote,[67] S. Grunewald,[35] P. Gruning,[25] G. M. Guidi,[71,72] H. K. Gulati,[106] Y. Guo,[36] A. Gupta,[86] M. K. Gupta,[106] E. K. Gustafson,[1] R. Gustafson,[125] L. Haegel,[98] O. Halim,[15,14] B. R. Hall,[68] E. D. Hall,[12] E. Z. Hamilton,[67] G. Hammond,[43] M. Haney,[65] M. M. Hanke,[8,9] J. Hanks,[44] C. Hanna,[86] O. A. Hannuksela,[90] J. Hanson,[7] T. Hardwick,[2] K. Haris,[16] J. Harms,[14,15] G. M. Harry,[126] I. W. Harry,[35] C.-J. Haster,[117] K. Haughian,[43] F. J. Hayes,[43] J. Healy,[57] A. Heidmann,[70] M. C. Heintze,[7] H. Heitmann,[64] P. Hello,[25] G. Hemming,[28] M. Hendry,[43] I. S. Heng,[43] J. Hennig,[8,9] A. W. Heptonstall,[1] Francisco Hernandez Vivanco,[6] M. Heurs,[8,9] S. Hild,[43] T. Hinderer,[127,36,128] D. Hoak,[28] S. Hochheim,[8,9] D. Hofman,[22] A. M. Holgado,[17] N. A. Holland,[21] K. Holt,[7] D. E. Holz,[89] P. Hopkins,[67] C. Horst,[23] J. Hough,[43] E. J. Howell,[62] C. G. Hoy,[67] A. Hreibi,[64] E. A. Huerta,[17] D. Huet,[25] B. Hughey,[33] M. Hulko,[1] S. Husa,[98] S. H. Huttner,[43] T. Huynh-Dinh,[7] B. Idzkowski,[73] A. Iess,[29,30] C. Ingram,[54] R. Inta,[83] G. Intini,[112,31] B. Irwin,[114] H. N. Isa,[43] J.-M. Isac,[70] M. Isi,[1] B. R. Iyer,[16] K. Izumi,[44] T. Jacqmin,[70] S. J. Jadhav,[129] K. Jani,[76] N. N. Janthalur,[129] P. Jaranowski,[130] A. C. Jenkins,[131] J. Jiang,[47] D. S. Johnson,[17] A. W. Jones,[11] D. I. Jones,[132] R. Jones,[43] R. J. G. Jonker,[36] L. Ju,[62] J. Junker,[8,9] C. V. Kalaghatgi,[67] V. Kalogera,[58] B. Kamai,[1] S. Kandhasamy,[84] G. Kang,[37] J. B. Kanner,[1] S. J. Kapadia,[23] S. Karki,[69] K. S. Karvinen,[8,9] R. Kashyap,[16] M. Kasprzack,[1] S. Katsanevas,[28] E. Katsavounidis,[12] W. Katzman,[7] S. Kaufer,[9] K. Kawabe,[44] N. V. Keerthana,[3] F. Kéfélian,[64] D. Keitel,[43] R. Kennedy,[107] J. S. Key,[133] F. Y. Khalili,[61] H. Khan,[26] I. Khan,[14,30] S. Khan,[8,9] Z. Khan,[106] E. A. Khazanov,[134] M. Khursheed,[60] N. Kijbunchoo,[21] Chunglee Kim,[135] J. C. Kim,[136] K. Kim,[90] W. Kim,[54] W. S. Kim,[137] Y.-M. Kim,[138] C. Kimball,[58] E. J. King,[54] P. J. King,[44] M. Kinley-Hanlon,[126] R. Kirchhoff,[8,9] J. S. Kissel,[44] L. Kleybolte,[139] J. H. Klika,[23] S. Klimenko,[47] T. D. Knowles,[38] P. Koch,[8,9] S. M. Koehlenbeck,[8,9] G. Koekoek,[36,140] S. Koley,[36] V. Kondrashov,[1] A. Kontos,[12] N. Koper,[8,9] M. Korobko,[139] W. Z. Korth,[1] I. Kowalska,[73] D. B. Kozak,[1] V. Kringel,[8,9] N. Krishnendu,[141] A. Królak,[142,143] G. Kuehn,[8,9] A. Kumar,[129] P. Kumar,[144] R. Kumar,[106] S. Kumar,[16] L. Kuo,[87] A. Kutynia,[142] S. Kwang,[23] B. D. Lackey,[35] K. H. Lai,[90] T. L. Lam,[90] M. Landry,[44] B. B. Lane,[12] R. N. Lang,[145] J. Lange,[57] B. Lantz,[48] R. K. Lanza,[12] A. Lartaux-Vollard,[25] P. D. Lasky,[6] M. Laxen,[7] A. Lazzarini,[1] C. Lazzaro,[51] P. Leaci,[112,31] S. Leavey,[8,9] Y. K. Lecoeuche,[44] C. H. Lee,[92] H. K. Lee,[146] H. M. Lee,[147] H. W. Lee,[136] J. Lee,[91] K. Lee,[43] J. Lehmann,[8,9] A. Lenon,[38] N. Leroy,[25] N. Letendre,[32] Y. Levin,[6,97] J. Li,[82] K. J. L. Li,[90] T. G. F. Li,[90] X. Li,[45] F. Lin,[6] F. Linde,[36] S. D. Linker,[110] T. B. Littenberg,[148] J. Liu,[62] X. Liu,[23] R. K. L. Lo,[90,1] N. A. Lockerbie,[24] L. T. London,[67] A. Longo,[149,150] M. Lorenzini,[14,15] V. Loriette,[151] M. Lormand,[7] G. Losurdo,[19] J. D. Lough,[8,9] G. Lovelace,[26] M. E. Lower,[152] H. Lück,[9,8] D. Lumaca,[29,30] A. P. Lundgren,[153] R. Lynch,[12] Y. Ma,[45] R. Macas,[67] S. Macfoy,[24] M. MacInnis,[12] D. M. Macleod,[67] A. Macquet,[64] F. Magaña-Sandoval,[41] L. Magaña Zertuche,[84] R. M. Magee,[86] E. Majorana,[31] I. Maksimovic,[151] A. Malik,[60] N. Man,[64] V. Mandic,[42] V. Mangano,[43] G. L. Mansell,[44,12] M. Manske,[23,21] M. Mantovani,[28] F. Marchesoni,[49,40] F. Marion,[32] S. Márka,[97] Z. Márka,[97] C. Markakis,[10,17] A. S. Markosyan,[48] A. Markowitz,[1] E. Maros,[1] A. Marquina,[101] S. Marsat,[35] F. Martelli,[71,72] I. W. Martin,[43] R. M. Martin,[34] D. V. Martynov,[11] K. Mason,[12] E. Massera,[107] A. Masserot,[32] T. J. Massinger,[1] M. Masso-Reid,[43] S. Mastrogiovanni,[112,31] A. Matas,[42,35] F. Matichard,[1,12] L. Matone,[97] N. Mavalvala,[12] N. Mazumder,[68] J. J. McCann,[62] R. McCarthy,[44] D. E. McClelland,[21] S. McCormick,[7] L. McCuller,[12] S. C. McGuire,[154] J. McIver,[1] D. J. McManus,[21] T. McRae,[21] S. T. McWilliams,[38] D. Meacher,[86] G. D. Meadors,[6] M. Mehmet,[8,9] A. K. Mehta,[16] J. Meidam,[36] A. Melatos,[96] G. Mendell,[44] R. A. Mercer,[23] L. Mereni,[22] E. L. Merilh,[44] M. Merzougui,[64] S. Meshkov,[1] C. Messenger,[43] C. Messick,[86] R. Metzdorff,[70] P. M. Meyers,[96] H. Miao,[11] C. Michel,[22] H. Middleton,[96] E. E. Mikhailov,[155] L. Milano,[78,5] A. L. Miller,[47] A. Miller,[112,31] M. Millhouse,[52] J. C. Mills,[67] M. C. Milovich-Goff,[110] O. Minazzoli,[64,156] Y. Minenkov,[30] A. Mishkin,[47] C. Mishra,[157] T. Mistry,[107] S. Mitra,[3] V. P. Mitrofanov,[61] G. Mitselmakher,[47] R. Mittleman,[12] G. Mo,[93] D. Moffa,[114] K. Mogushi,[84] S. R. P. Mohapatra,[12] M. Montani,[71,72] C. J. Moore,[10] D. Moraru,[44] G. Moreno,[44] S. Morisaki,[81] B. Mours,[32] C. M. Mow-Lowry,[11] Arunava Mukherjee,[8,9] D. Mukherjee,[23] S. Mukherjee,[103] N. Mukund,[3] A. Mullavey,[7] J. Munch,[54] E. A. Muñiz,[41] M. Muratore,[33] P. G. Murray,[43,158,159] I. Nardecchia,[29,30] L. Naticchioni,[112,31] R. K. Nayak,[160] J. Neilson,[110] G. Nelemans,[63,36] T. J. N. Nelson,[7] M. Nery,[8,9] A. Neunzert,[125] K. Y. Ng,[12] S. Ng,[54] P. Nguyen,[69] D. Nichols,[127,36] S. Nissanke,[127,36] F. Nocera,[28] C. North,[67] L. K. Nuttall,[153] M. Obergaulinger,[20] J. Oberling,[44] B. D. O'Brien,[47] G. D. O'Dea,[110] G. H. Ogin,[161] J. J. Oh,[137] S. H. Oh,[137] F. Ohme,[8,9] H. Ohta,[81] M. A. Okada,[13] M. Oliver,[98] P. Oppermann,[8,9] Richard J. Oram,[7] B. O'Reilly,[7] R. G. Ormiston,[42] L. F. Ortega,[47] R. O'Shaughnessy,[57] S. Ossokine,[35] D. J. Ottaway,[54] H. Overmier,[7] B. J. Owen,[83] A. E. Pace,[86] G. Pagano,[18,19] M. A. Page,[62] A. Pai,[121] S. A. Pai,[60] J. R. Palamos,[69] O. Palashov,[134] C. Palomba,[31] A. Pal-Singh,[139] Huang-Wei Pan,[87] B. Pang,[45] P. T. H. Pang,[90] C. Pankow,[58] F. Pannarale,[112,31]

B. C. Pant,[60] F. Paoletti,[19] A. Paoli,[28] A. Parida,[3] W. Parker,[7,154] D. Pascucci,[43] A. Pasqualetti,[28] R. Passaquieti,[18,19] D. Passuello,[19] M. Patil,[143] B. Patricelli,[18,19] B. L. Pearlstone,[43] C. Pedersen,[67] M. Pedraza,[1] R. Pedurand,[22,162] A. Pele,[7] S. Penn,[163] C. J. Perez,[44] A. Perreca,[111,95] H. P. Pfeiffer,[35,117] M. Phelps,[8,9] K. S. Phukon,[3] O. J. Piccinni,[112,31] M. Pichot,[64] F. Piergiovanni,[71,72] G. Pillant,[28] L. Pinard,[22] M. Pirello,[44] M. Pitkin,[43] R. Poggiani,[18,19] D. Y. T. Pong,[90] S. Ponrathnam,[3] P. Popolizio,[28] E. K. Porter,[27] J. Powell,[152] A. K. Prajapati,[106] J. Prasad,[3] K. Prasai,[48] R. Prasanna,[129] G. Pratten,[98] T. Prestegard,[23] S. Privitera,[35] G. A. Prodi,[111,95] L. G. Prokhorov,[61] O. Puncken,[8,9] M. Punturo,[40] P. Puppo,[31] M. Pürrer,[35] H. Qi,[23] V. Quetschke,[103] P. J. Quinonez,[33] E. A. Quintero,[1] R. Quitzow-James,[69] F. J. Raab,[44] H. Radkins,[44] N. Radulescu,[64] P. Raffai,[105] S. Raja,[60] C. Rajan,[60] B. Rajbhandari,[83] M. Rakhmanov,[103] K. E. Ramirez,[103] A. Ramos-Buades,[98] Javed Rana,[3] K. Rao,[58] P. Rapagnani,[112,31] V. Raymond,[67] M. Razzano,[18,19] J. Read,[26] T. Regimbau,[32] L. Rei,[59] S. Reid,[24] D. H. Reitze,[1,47] W. Ren,[17] F. Ricci,[112,31] C. J. Richardson,[33] J. W. Richardson,[1] P. M. Ricker,[17] K. Riles,[125] M. Rizzo,[58] N. A. Robertson,[1,43] R. Robie,[43] F. Robinet,[25] A. Rocchi,[30] L. Rolland,[32] J. G. Rollins,[1] V. J. Roma,[69] M. Romanelli,[66] R. Romano,[4,5] C. L. Romel,[44] J. H. Romie,[7] K. Rose,[114] D. Rosińska,[164,53] S. G. Rosofsky,[17] M. P. Ross,[165] S. Rowan,[43] A. Rüdiger,[8,9,†] P. Ruggi,[28] G. Rutins,[166] K. Ryan,[44] S. Sachdev,[1] T. Sadecki,[44] M. Sakellariadou,[131] L. Salconi,[28] M. Saleem,[141] A. Samajdar,[36] L. Sammut,[6] E. J. Sanchez,[1] L. E. Sanchez,[1] N. Sanchis-Gual,[20] V. Sandberg,[44] J. R. Sanders,[41] K. A. Santiago,[34] N. Sarin,[6] B. Sassolas,[22,67] P. R. Saulson,[41] O. Sauter,[125] R. L. Savage,[44] P. Schale,[69] M. Scheel,[45] J. Scheuer,[58] P. Schmidt,[63] R. Schnabel,[139] R. M. S. Schofield,[69] A. Schönbeck,[139] E. Schreiber,[8,9] B. W. Schulte,[8,9] B. F. Schutz,[67] S. G. Schwalbe,[33] J. Scott,[43] S. M. Scott,[21] E. Seidel,[17] D. Sellers,[7] A. S. Sengupta,[167] N. Sennett,[35] D. Sentenac,[28] V. Sequino,[29,30,14] A. Sergeev,[134] Y. Setyawati,[8,9] D. A. Shaddock,[21] T. Shaffer,[44] M. S. Shahriar,[58] M. B. Shaner,[110] L. Shao,[35] P. Sharma,[60] P. Shawhan,[75] H. Shen,[17] R. Shink,[168] D. H. Shoemaker,[12] D. M. Shoemaker,[76] S. ShyamSundar,[60] K. Siellez,[76] M. Sieniawska,[53] D. Sigg,[44] A. D. Silva,[13] L. P. Singer,[79] N. Singh,[73] A. Singhal,[14,31] A. M. Sintes,[98] S. Sitmukhambetov,[103] V. Skliris,[67] B. J. J. Slagmolen,[21] T. J. Slaven-Blair,[62] J. R. Smith,[26] R. J. E. Smith,[6] S. Somala,[169] E. J. Son,[137] B. Sorazu,[43] F. Sorrentino,[59] T. Souradeep,[3] E. Sowell,[83] A. P. Spencer,[43] A. K. Srivastava,[106] V. Srivastava,[41] K. Staats,[58] C. Stachie,[64] M. Standke,[8,9] D. A. Steer,[27] M. Steinke,[8,9] J. Steinlechner,[139,43] S. Steinlechner,[139] D. Steinmeyer,[8,9] S. P. Stevenson,[152] D. Stocks,[48] R. Stone,[103] D. J. Stops,[11] K. A. Strain,[43] G. Stratta,[71,72] S. E. Strigin,[61] A. Strunk,[44] R. Sturani,[170] A. L. Stuver,[171] V. Sudhir,[12] T. Z. Summerscales,[172] L. Sun,[1] S. Sunil,[106] J. Suresh,[3] P. J. Sutton,[67] B. L. Swinkels,[36] M. J. Szczepańczyk,[33] M. Tacca,[36] S. C. Tait,[43] C. Talbot,[6] D. Talukder,[69] D. B. Tanner,[47] M. Tápai,[122] A. Taracchini,[35] J. D. Tasson,[93] R. Taylor,[1] F. Thies,[8,9] M. Thomas,[7] P. Thomas,[44] S. R. Thondapu,[60] K. A. Thorne,[7] E. Thrane,[6] Shubhanshu Tiwari,[111,95] Srishti Tiwari,[123] V. Tiwari,[67] K. Toland,[43] M. Tonelli,[18,19] Z. Tornasi,[43] A. Torres-Forné,[173] C. I. Torrie,[1] D. Töyrä,[11] F. Travasso,[28,40] G. Traylor,[7] M. C. Tringali,[73] A. Trovato,[27] L. Trozzo,[174,19] R. Trudeau,[1] K. W. Tsang,[36] M. Tse,[12] R. Tso,[45] L. Tsukada,[81] D. Tsuna,[81] D. Tuyenbayev,[103] K. Ueno,[81] D. Ugolini,[175] C. S. Unnikrishnan,[123] A. L. Urban,[2] S. A. Usman,[67] H. Vahlbruch,[9] G. Vajente,[1] G. Valdes,[2] N. van Bakel,[36] M. van Beuzekom,[36] J. F. J. van den Brand,[74,36] C. Van Den Broeck,[36,176] D. C. Vander-Hyde,[41] J. V. van Heijningen,[62] L. van der Schaaf,[36] A. A. van Veggel,[43] M. Vardaro,[50,51] V. Varma,[45] S. Vass,[1] M. Vasúth,[46] A. Vecchio,[11] G. Vedovato,[51] J. Veitch,[43] P. J. Veitch,[54] K. Venkateswara,[165] G. Venugopalan,[1] D. Verkindt,[32] F. Vetrano,[71,72] A. Viceré,[71,72] A. D. Viets,[23] D. J. Vine,[166] J.-Y. Vinet,[64] S. Vitale,[12] T. Vo,[41] H. Vocca,[39,40] C. Vorvick,[44] S. P. Vyatchanin,[61] A. R. Wade,[1] L. E. Wade,[114] M. Wade,[114] R. Walet,[36] M. Walker,[26] L. Wallace,[1] S. Walsh,[23] G. Wang,[14,19] H. Wang,[11] J. Z. Wang,[125] W. H. Wang,[103] Y. F. Wang,[90] R. L. Ward,[21] Z. A. Warden,[33] J. Warner,[44] M. Was,[32] J. Watchi,[99] B. Weaver,[44] L.-W. Wei,[8,9] M. Weinert,[8,9] A. J. Weinstein,[1] R. Weiss,[12] F. Wellmann,[8,9] L. Wen,[62] E. K. Wessel,[17] P. Weßels,[8,9] J. W. Westhouse,[33] K. Wette,[21] J. T. Whelan,[57] B. F. Whiting,[47] C. Whittle,[12] D. M. Wilken,[8,9] D. Williams,[43] A. R. Williamson,[127,36] J. L. Willis,[1] B. Willke,[8,9] M. H. Wimmer,[8,9] W. Winkler,[8,9] C. C. Wipf,[1] H. Wittel,[8,9] G. Woan,[43] J. Woehler,[8,9] J. K. Wofford,[57] J. Worden,[44] J. L. Wright,[43] D. S. Wu,[8,9] D. M. Wysocki,[57] L. Xiao,[1] H. Yamamoto,[1] C. C. Yancey,[75] L. Yang,[113] M. J. Yap,[21] M. Yazback,[47] D. W. Yeeles,[67] Hang Yu,[12] Haocun Yu,[12] S. H. R. Yuen,[90] M. Yvert,[32] A. K. Zadrożny,[103,142] M. Zanolin,[33] T. Zelenova,[28] J.-P. Zendri,[51] M. Zevin,[58] J. Zhang,[62] L. Zhang,[1] T. Zhang,[43] C. Zhao,[62] M. Zhou,[58] Z. Zhou,[58] X. J. Zhu,[6] M. E. Zucker,[1,12] J. Zweizig,[1] M. Keith,[177] M. Kerr,[178] L. Kuiper,[179] A. K. Harding,[180] A. Lyne,[177] J. Palfreyman,[181] B. Stappers,[177] and P. Weltervrede[177]

(LIGO Scientific Collaboration and Virgo Collaboration)

[1]LIGO, California Institute of Technology, Pasadena, California 91125, USA
[2]Louisiana State University, Baton Rouge, Louisiana 70803, USA
[3]Inter-University Centre for Astronomy and Astrophysics, Pune 411007, India
[4]Università di Salerno, Fisciano, I-84084 Salerno, Italy
[5]INFN, Sezione di Napoli, Complesso Universitario di Monte S.Angelo, I-80126 Napoli, Italy
[6]OzGrav, School of Physics & Astronomy, Monash University, Clayton 3800, Victoria, Australia
[7]LIGO Livingston Observatory, Livingston, Louisiana 70754, USA
[8]Max Planck Institute for Gravitational Physics (Albert Einstein Institute), D-30167 Hannover, Germany
[9]Leibniz Universität Hannover, D-30167 Hannover, Germany
[10]University of Cambridge, Cambridge CB2 1TN, United Kingdom
[11]University of Birmingham, Birmingham B15 2TT, United Kingdom
[12]LIGO, Massachusetts Institute of Technology, Cambridge, Massachusetts 02139, USA
[13]Instituto Nacional de Pesquisas Espaciais, 12227-010 São José dos Campos, São Paulo, Brazil
[14]Gran Sasso Science Institute (GSSI), I-67100L'Aquila, Italy
[15]INFN, Laboratori Nazionali del Gran Sasso, I-67100 Assergi, Italy
[16]International Centre for Theoretical Sciences, Tata Institute of Fundamental Research, Bengaluru 560089, India
[17]NCSA, University of Illinois at Urbana-Champaign, Urbana, Illinois 61801, USA
[18]Università di Pisa, I-56127 Pisa, Italy
[19]INFN, Sezione di Pisa, I-56127 Pisa, Italy
[20]Departamento de Astronomía y Astrofísica, Universitat de València, E-46100 Burjassot, València, Spain
[21]OzGrav, Australian National University, Canberra, Australian Capital Territory 0200, Australia
[22]Laboratoire des Matériaux Avancés (LMA), CNRS/IN2P3, F-69622 Villeurbanne, France
[23]University of Wisconsin-Milwaukee, Milwaukee, Wisconsin 53201, USA
[24]SUPA, University of Strathclyde, Glasgow G1 1XQ, United Kingdom
[25]LAL, Univ. Paris-Sud, CNRS/IN2P3, Université Paris-Saclay, F-91898 Orsay, France
[26]California State University Fullerton, Fullerton, California 92831, USA
[27]APC, AstroParticule et Cosmologie, Université Paris Diderot, CNRS/IN2P3, CEA/Irfu, Observatoire de Paris, Sorbonne Paris Cité, F-75205 Paris Cedex 13, France
[28]European Gravitational Observatory (EGO), I-56021 Cascina, Pisa, Italy
[29]Università di Roma Tor Vergata, I-00133 Roma, Italy
[30]INFN, Sezione di Roma Tor Vergata, I-00133 Roma, Italy
[31]INFN, Sezione di Roma, I-00185 Roma, Italy
[32]Laboratoire d'Annecy de Physique des Particules (LAPP), Univ. Grenoble Alpes, Université Savoie Mont Blanc, CNRS/IN2P3, F-74941 Annecy, France
[33]Embry-Riddle Aeronautical University, Prescott, Arizona 86301, USA
[34]Montclair State University, Montclair, New Jersey 07043, USA
[35]Max Planck Institute for Gravitational Physics (Albert Einstein Institute), D-14476 Potsdam-Golm, Germany
[36]Nikhef, Science Park 105, 1098 XG Amsterdam, Netherlands
[37]Korea Institute of Science and Technology Information, Daejeon 34141, South Korea
[38]West Virginia University, Morgantown, West Virginia 26506, USA
[39]Università di Perugia, I-06123 Perugia, Italy
[40]INFN, Sezione di Perugia, I-06123 Perugia, Italy
[41]Syracuse University, Syracuse, New York 13244, USA
[42]University of Minnesota, Minneapolis, Minnesota 55455, USA
[43]SUPA, University of Glasgow, Glasgow G12 8QQ, United Kingdom
[44]LIGO Hanford Observatory, Richland, Washington, D.C. 99352, USA
[45]Caltech CaRT, Pasadena, California 91125, USA
[46]Wigner RCP, RMKI, H-1121 Budapest, Konkoly Thege Miklós út 29-33, Hungary
[47]University of Florida, Gainesville, Florida 32611, USA
[48]Stanford University, Stanford, California 94305, USA
[49]Università di Camerino, Dipartimento di Fisica, I-62032 Camerino, Italy
[50]Università di Padova, Dipartimento di Fisica e Astronomia, I-35131 Padova, Italy
[51]INFN, Sezione di Padova, I-35131 Padova, Italy
[52]Montana State University, Bozeman, Montana 59717, USA
[53]Nicolaus Copernicus Astronomical Center, Polish Academy of Sciences, 00-716, Warsaw, Poland
[54]OzGrav, University of Adelaide, Adelaide, South Australia 5005, Australia
[55]Theoretisch-Physikalisches Institut, Friedrich-Schiller-Universität Jena, D-07743 Jena, Germany
[56]INFN, Sezione di Milano Bicocca, Gruppo Collegato di Parma, I-43124 Parma, Italy

[57]*Rochester Institute of Technology, Rochester, New York 14623, USA*
[58]*Center for Interdisciplinary Exploration & Research in Astrophysics (CIERA), Northwestern University, Evanston, Illinois 60208, USA*
[59]*INFN, Sezione di Genova, I-16146 Genova, Italy*
[60]*RRCAT, Indore, Madhya Pradesh 452013, India*
[61]*Faculty of Physics, Lomonosov Moscow State University, Moscow 119991, Russia*
[62]*OzGrav, University of Western Australia, Crawley, Western Australia 6009, Australia*
[63]*Department of Astrophysics/IMAPP, Radboud University Nijmegen, P.O. Box 9010, 6500 GL Nijmegen, Netherlands*
[64]*Artemis, Université Côte d'Azur, Observatoire Côte d'Azur, CNRS, CS 34229, F-06304 Nice Cedex 4, France*
[65]*Physik-Institut, University of Zurich, Winterthurerstrasse 190, 8057 Zurich, Switzerland*
[66]*Univ Rennes, CNRS, Institut FOTON-UMR6082, F-3500 Rennes, France*
[67]*Cardiff University, Cardiff CF24 3AA, United Kingdom*
[68]*Washington State University, Pullman, Washington, D.C. 99164, USA*
[69]*University of Oregon, Eugene, Oregon 97403, USA*
[70]*Laboratoire Kastler Brossel, Sorbonne Université, CNRS, ENS-Université PSL, Collège de France, F-75005 Paris, France*
[71]*Università degli Studi di Urbino 'Carlo Bo,' I-61029 Urbino, Italy*
[72]*INFN, Sezione di Firenze, I-50019 Sesto Fiorentino, Firenze, Italy*
[73]*Astronomical Observatory Warsaw University, 00-478 Warsaw, Poland*
[74]*VU University Amsterdam, 1081 HV Amsterdam, Netherlands*
[75]*University of Maryland, College Park, Maryland 20742, USA*
[76]*School of Physics, Georgia Institute of Technology, Atlanta, Georgia 30332, USA*
[77]*Université Claude Bernard Lyon 1, F-69622 Villeurbanne, France*
[78]*Università di Napoli "Federico II," Complesso Universitario di Monte S.Angelo, I-80126 Napoli, Italy*
[79]*NASA Goddard Space Flight Center, Greenbelt, Maryland 20771, USA*
[80]*Dipartimento di Fisica, Università degli Studi di Genova, I-16146 Genova, Italy*
[81]*RESCEU, University of Tokyo, Tokyo, 113-0033, Japan*
[82]*Tsinghua University, Beijing 100084, China*
[83]*Texas Tech University, Lubbock, Texas 79409, USA*
[84]*The University of Mississippi, University, Mississippi 38677, USA*
[85]*Museo Storico della Fisica e Centro Studi e Ricerche "Enrico Fermi," I-00184 Roma, Italyrico Fermi, I-00184 Roma, Italy*
[86]*The Pennsylvania State University, University Park, Pennsylvania 16802, USA*
[87]*National Tsing Hua University, Hsinchu City, 30013 Taiwan, Republic of China*
[88]*Charles Sturt University, Wagga Wagga, New South Wales 2678, Australia*
[89]*University of Chicago, Chicago, Illinois 60637, USA*
[90]*The Chinese University of Hong Kong, Shatin, NT, Hong Kong*
[91]*Seoul National University, Seoul 08826, South Korea*
[92]*Pusan National University, Busan 46241, South Korea*
[93]*Carleton College, Northfield, Minnesota 55057, USA*
[94]*INAF, Osservatorio Astronomico di Padova, I-35122 Padova, Italy*
[95]*INFN, Trento Institute for Fundamental Physics and Applications, I-38123 Povo, Trento, Italy*
[96]*OzGrav, University of Melbourne, Parkville, Victoria 3010, Australia*
[97]*Columbia University, New York, New York 10027, USA*
[98]*Universitat de les Illes Balears, IAC3—IEEC, E-07122 Palma de Mallorca, Spain*
[99]*Université Libre de Bruxelles, Brussels 1050, Belgium*
[100]*Sonoma State University, Rohnert Park, California 94928, USA*
[101]*Departamento de Matemáticas, Universitat de València, E-46100 Burjassot, València, Spain*
[102]*University of Rhode Island, Kingston, Rhode Island 02881, USA*
[103]*The University of Texas Rio Grande Valley, Brownsville, Texas 78520, USA*
[104]*Bellevue College, Bellevue, Washington, D.C. 98007, USA*
[105]*MTA-ELTE Astrophysics Research Group, Institute of Physics, Eötvös University, Budapest 1117, Hungary*
[106]*Institute for Plasma Research, Bhat, Gandhinagar 382428, India*
[107]*The University of Sheffield, Sheffield S10 2TN, United Kingdom*
[108]*IGFAE, Campus Sur, Universidade de Santiago de Compostela, 15782 Spain*

[109]*Dipartimento di Scienze Matematiche, Fisiche e Informatiche, Università di Parma, I-43124 Parma, Italy*
[110]*California State University, Los Angeles, 5151 State University Drive, Los Angeles, California 90032, USA*
[111]*Università di Trento, Dipartimento di Fisica, I-38123 Povo, Trento, Italy*
[112]*Università di Roma 'La Sapienza,' I-00185 Roma, Italy*
[113]*Colorado State University, Fort Collins, Colorado 80523, USA*
[114]*Kenyon College, Gambier, Ohio 43022, USA*
[115]*Christopher Newport University, Newport News, Virginia 23606, USA*
[116]*National Astronomical Observatory of Japan, 2-21-1 Osawa, Mitaka, Tokyo 181-8588, Japan*
[117]*Canadian Institute for Theoretical Astrophysics, University of Toronto, Toronto, Ontario M5S 3H8, Canada*
[118]*Observatori Astronòmic, Universitat de València, E-46980 Paterna, València, Spain*
[119]*School of Mathematics, University of Edinburgh, Edinburgh EH9 3FD, United Kingdom*
[120]*Institute Of Advanced Research, Gandhinagar 382426, India*
[121]*Indian Institute of Technology Bombay, Powai, Mumbai 400 076, India*
[122]*University of Szeged, Dóm tér 9, Szeged 6720, Hungary*
[123]*Tata Institute of Fundamental Research, Mumbai 400005, India*
[124]*INAF, Osservatorio Astronomico di Capodimonte, I-80131, Napoli, Italy*
[125]*University of Michigan, Ann Arbor, Michigan 48109, USA*
[126]*American University, Washington, D.C. 20016, USA*
[127]*GRAPPA, Anton Pannekoek Institute for Astronomy and Institute of High-Energy Physics, University of Amsterdam, Science Park 904, 1098 XH Amsterdam, Netherlands*
[128]*Delta Institute for Theoretical Physics, Science Park 904, 1090 GL Amsterdam, Netherlands*
[129]*Directorate of Construction, Services & Estate Management, Mumbai 400094 India*
[130]*University of Białystok, 15-424 Białystok, Poland*
[131]*King's College London, University of London, London WC2R 2LS, United Kingdom*
[132]*University of Southampton, Southampton SO17 1BJ, United Kingdom*
[133]*University of Washington Bothell, Bothell, Washington, D.C. 98011, USA*
[134]*Institute of Applied Physics, Nizhny Novgorod, 603950, Russia*
[135]*Ewha Womans University, Seoul 03760, South Korea*
[136]*Inje University Gimhae, South Gyeongsang 50834, South Korea*
[137]*National Institute for Mathematical Sciences, Daejeon 34047, South Korea*
[138]*Ulsan National Institute of Science and Technology, Ulsan 44919, South Korea*
[139]*Universität Hamburg, D-22761 Hamburg, Germany*
[140]*Maastricht University, P.O. Box 616, 6200 MD Maastricht, Netherlands*
[141]*Chennai Mathematical Institute, Chennai 603103, India*
[142]*NCBJ, 05-400 Świerk-Otwock, Poland*
[143]*Institute of Mathematics, Polish Academy of Sciences, 00656 Warsaw, Poland*
[144]*Cornell University, Ithaca, New York 14850, USA*
[145]*Hillsdale College, Hillsdale, Michigan 49242, USA*
[146]*Hanyang University, Seoul 04763, South Korea*
[147]*Korea Astronomy and Space Science Institute, Daejeon 34055, South Korea*
[148]*NASA Marshall Space Flight Center, Huntsville, Alabama 35811, USA*
[149]*Dipartimento di Matematica e Fisica, Università degli Studi Roma Tre, I-00146 Roma, Italy*
[150]*INFN, Sezione di Roma Tre, I-00146 Roma, Italy*
[151]*ESPCI, CNRS, F-75005 Paris, France*
[152]*OzGrav, Swinburne University of Technology, Hawthorn VIC 3122, Australia*
[153]*University of Portsmouth, Portsmouth, PO1 3FX, United Kingdom*
[154]*Southern University and A&M College, Baton Rouge, Louisiana 70813, USA*
[155]*College of William and Mary, Williamsburg, Virginia 23187, USA*
[156]*Centre Scientifique de Monaco, 8 quai Antoine Ier, MC-98000, Monaco*
[157]*Indian Institute of Technology Madras, Chennai 600036, India*
[158]*INFN Sezione di Torino, Via P. Giuria 1, I-10125 Torino, Italy*
[159]*Institut des Hautes Etudes Scientifiques, F-91440 Bures-sur-Yvette, France*
[160]*IISER-Kolkata, Mohanpur, West Bengal 741252, India*
[161]*Whitman College, 345 Boyer Avenue, Walla Walla, Washington, D.C. 99362 USA*
[162]*Université de Lyon, F-69361 Lyon, France*
[163]*Hobart and William Smith Colleges, Geneva, New York 14456, USA*
[164]*Janusz Gil Institute of Astronomy, University of Zielona Góra, 65-265 Zielona Góra, Poland*

[165]*University of Washington, Seattle, Washington, D.C. 98195, USA*
[166]*SUPA, University of the West of Scotland, Paisley PA1 2BE, United Kingdom*
[167]*Indian Institute of Technology, Gandhinagar Ahmedabad Gujarat 382424, India*
[168]*Université de Montréal/Polytechnique, Montreal, Quebec H3T 1J4, Canada*
[169]*Indian Institute of Technology Hyderabad, Sangareddy, Khandi, Telangana 502285, India*
[170]*International Institute of Physics, Universidade Federal do Rio Grande do Norte, Natal RN 59078-970, Brazil*
[171]*Villanova University, 800 Lancaster Avenue, Villanova, Pennsylvania 19085, USA*
[172]*Andrews University, Berrien Springs, Michigan 49104, USA*
[173]*Max Planck Institute for Gravitationalphysik (Albert Einstein Institute), D-14476 Potsdam-Golm, Germany*
[174]*Università di Siena, I-53100 Siena, Italy*
[175]*Trinity University, San Antonio, Texas 78212, USA*
[176]*Van Swinderen Institute for Particle Physics and Gravity, University of Groningen, Nijenborgh 4, 9747 AG Groningen, Netherlands*
[177]*School of Physics and Astronomy, University of Manchester, Manchester, M13 9PL, United Kingdom*
[178]*Space Science Division, Naval Research Laboratory, Washington, D.C. 20375-5352, USA*
[179]*SRON-Netherlands Institute for Space Research, Sorbonnelaan 2, NL-3584 CA Utrecht, Netherlands*
[180]*Astrophysics Science Division, NASA Goddard Space Flight Center, Greenbelt, Maryland 20771, USA*
[181]*Department of Physical Sciences, University of Tasmania, Private Bag 37, Hobart, Tasmania 7001, Australia*

[†]Deceased.